Climate Data Record (CDR) Program

Climate Algorithm Theoretical Basis Document (C-ATBD)

Sea Ice Concentration

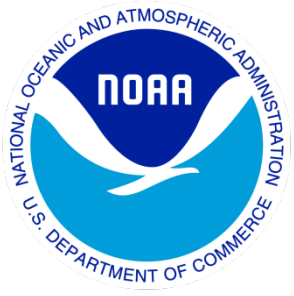

CDR Program Document Number: CDRP-ATBD-0107
Configuration Item Number: 01B-11 and 01B-11a
Revision 7 / March 6, 2018

REVISION HISTORY

Rev.	Author	DSR No.	Description	Date
1	Walt Meier, Research Scientist, NSIDC	DSR-112	Initial release.	09/20/2011
2	Walt Meier, Research Scientist, NSIDC	DSR-204	Added description of monthly files and memory allocations for processing. Sections 3.2, 3.4.4, and 5.6.	05/29/2012
3	Walt Meier, Research Scientist, NSIDC	DSR-411	Changes made to describe Version 2 Revision 0 of the CDR. Sections 3.2, 3.3.1, 3.4.1.4, 3.4.4.1, 3.4.4.2, and 5.6. 6.1.4 (deleted)	03/26/2013
4	Ann Windnagel, Professional Research Assistant, NSIDC	DSR-920	Changes made to describe Version 2 Revision 1 of the CDR. Updated Figures 2 and 5 in Section 3.2, Sections 1.3 and 5.6, and Table 12.	09/19/2015
5	Ann Windnagel, Professional Research Assistant, NSIDC	DSR-1148	Changes made to describe Version 3 and the near-real-time portion of the time series: Updated sections 1.1, 2.1, 2.2, 3, 4, 5.6, 6, and 8.	09/14/2017
6	Ann Windnagel, Professional Research Assistant, NSIDC	DSR-1216	Changes made to describe Version 3 Revision 1. Updated sections 3.2, 3.3, and 3.4. Changes made to address Version 3.1: Updated section 3.3.1.	12/20/2017
7	Ann Windnagel, Professional Research Assistant, NSIDC	DSR-1240	Changes made to tables 3, 4, and 5: instruments for the input data were changed from SMMIS and SMM/I to SSMIS and SSM/I.	03/06/2018

TABLE of CONTENTS

LIST of FIGURES

LIST of TABLES

ACRONYMS AND ABBREVIATIONS

Acronym or Abbreviation	Meaning
BT	Bootstrap
CATBD	Climate Algorithm Theoretical Basis Document
CDR	Climate Data Record
CLASS	Comprehensive Large Array-data Stewardship System
DAAC	Distributed Active Archive Center
DMSP	Defense Meteorological Satellite Program
DOY	Day of Year
IFOV	Instantaneous Field of View
FY	First Year
GSFC	Goddard Space Flight Center
H	Horizontal
ICDR	Interim Climate Data Record
MY	Multi-year
NAS	National Academies of Science
NASA	National Aeronautics and Space Administration
NCDC	National Climatic Data Center
NOAA	National Oceanic and Atmospheres Administration
NSIDC	National Snow and Ice Data Center
NRT	Near Real Time
NT	NASA Team
OW	Open Water
QC	Quality Control
RSS	Remote Sensing Systems, Inc.
SMMR	Scanning Multichannel Microwave Radiometer
SSM/I	Special Sensor Microwave Imager
SSMIS	Special Sensor Microwave Imager/Sounder
SST	Sea Surface Temperature
TCDR	Thematic Climate Data Record
V	Vertical

1. Introduction

1.1 Purpose

The purpose of this document is to describe the sea ice CDR algorithm (Meier et al. 2014; Peng et al. 2013). Beginning in 2015, updates are submitted to the National Centers for Environmental Information by Florence Fetterer at the National Snow and Ice Data Center (NSIDC). The algorithm is used to create the Sea Ice Concentration Climate Data Record (CDR), using the Special Sensor Microwave/Imager (SSM/I) and Special Sensor Microwave Imager and Sounder (SSMIS) sensors on U.S. Department of Defense Meteorological Satellite Program (DMSP) platforms. The goal of the Sea Ice Concentration CDR is to provide a consistent, reliable, and well-documented product that meets CDR guidelines as defined in Climate data records from environmental satellites (NAS, 2004). This product is supplied in two parts. A final product that is created from quality controlled input data available from NSIDC as the NOAA/NSIDC Climate Data Record of Passive Microwave Sea Ice Concentration (https://nsidc.org/data/g02202), and a near-real-time provisional product that is created from provisional input data available from NSIDC as the Near-Real-Time NOAA/NSIDC Climate Data Record of Passive Microwave Sea Ice Concentration (https://nsidc.org/data/g10016). The near-real-time provisional product is provided to users until the release of the finalized Sea Ice Concentration CDR (NOAA data set ID 01B-11, NSIDC data set ID G02202), which is available at an approximately one-year latency

The actual algorithm is defined in the computer program (code) that accompanies this document; and thus, the intent here is to provide a guide to understanding that algorithm, from both a scientific perspective and a software engineering perspective in order to assist in evaluation of the code. In the finalized portion of this product, ancillary fields of sea ice concentration produced at NASA Goddard Space Flight Center (GSFC) are also included because they employ manual corrections by Goddard scientists and extend the time series to encompass the Nimbus-7 Scanning Multichannel Microwave Radiometer (SMMR) era (1978-1987). The near-real-time provisional portion of this product does not contain those ancillary products.

1.2 Definitions

Following is a summary of the symbols used to define the algorithm.

$$T_B = brightness\ temperature = \varepsilon * T \quad (1)$$

$$\varepsilon = emissivity \quad (2)$$

$$T = physical\ temperature \quad (3)$$

$$PR = polarization\ ratio \quad (4)$$

GR = gradient ratio *(5)*

1.3 Referencing this Document

This document should be referenced as follows:

Sea Ice Concentration - Climate Algorithm Theoretical Basis Document, NOAA Climate Data Record Program CDRP-ATBD-0107 Rev. 5 (2017). Available at https://www.ncdc.noaa.gov/cdr/oceanic/sea-ice-concentration

1.4 Document Maintenance

This is the ATBD for the Sea Ice Concentration Climate Data Record, Version 3, Revision 0 and the Near-Real-Time Sea Ice Concentration Climate Data Record, Version 1, Revision 0. The source code is used to create both products.

2. Observing Systems Overview

2.1 Products Generated

The primary generated product is the Sea Ice Concentration climate data record based on gridded brightness temperatures (T_Bs) from the DMSP series of SSM/I and SSMIS passive microwave radiometers. The concentration CDR is an estimate of sea ice concentration that is produced by combining concentration estimates from two algorithms developed at the NASA Goddard Space Flight Center (GSFC): the NASA Team algorithm (Cavalieri et al., 1984) and the Bootstrap algorithm (Comiso, 1986). These algorithms are described in more detail in Section 3. For the finalized portion of this product, called the Thematic CDR (TCDR, NSIDC data set ID G02202), NSIDC uses each individual algorithm to process and combine swath brightness temperature data from Remote Sensing Systems, Inc. (RSS). For the near-real-time provisional portion of this product, called the Interim CDR (ICDR, NSIDC data set ID G10016), NSIDC uses each individual algorithm to process and combine swath brightness temperature data from the NOAA Comprehensive Large Array-Data Stewardship System (CLASS). See section 3 for more information on the input brightness temperatures.

Accompanying the concentration estimates are data quality information fields. One field is a concentration standard deviation that indicates spatial variability and the variability between the NASA Team and Bootstrap algorithm estimates. Grid cells with high standard deviations indicate values with lower confidence levels. Another field includes quality information such as melt state and proximity to the coast, regimes that tend to have higher errors.

In addition, for the TCDR product only, sea ice concentration fields produced by Goddard are provided for heritage users of older products. These include concentration products from the NASA Team algorithm (https://nsidc.org/data/nsidc-0051) and Bootstrap algorithm (https://nsidc.org/data/nsidc-0079) that NSIDC has been distributing for several years through the NASA Distributed Active Archive Center (DAAC). These data are processed almost identically to the data used in the CDR concentration estimates but are produced at NASA GSFC and include manual quality control. This hand editing removes spurious ice in grid cells that are not removed through automated filtering methods and any other bad data discovered through the manual inspection. However, the hand-editing process has not been documented and thus, is not traceable, which precludes it from being part of the CDR. In addition, older versions of the RSS brightness temperatures were used as inputs for some parts of the record, though these differences are small. Thus, while these products do not have full traceability, they do result in a better overall quality record. In addition, they also include sea ice estimates from the NASA Nimbus-7 SMMR sensor, which predates DMSP and extends the total time series to late 1978 with every-other-day concentration estimates. A merged field of the Goddard NASA Team and Bootstrap algorithm estimate is also provided as a longer-term analog of the DMSP SSM/I-SSMIS CDR. NSIDC creates this

merged product from the Goddard NASA Team and Bootstrap data using the same methodology as the CDR.

2.2 Instrument Characteristics

The first SSM/I sensor was launched aboard the DMSP-F8 mission in 1987 (Hollinger et al., 1987). A series of SSM/I conically-scanning sensors on subsequent DMSP satellites has provided a continuous data stream since then. However, only sensors on the DMSP-F8, -F11, -F13, -F17, and -F18 platforms are used in the generation of the CDR. The SSM/I sensor has seven channels at four frequencies. The 19.4, 37.0, and 85.5 GHz frequencies are dual polarized, horizontal (H) and vertical (V); the 22.2 GHz frequency has only a single vertically polarized channel. The 85.5 GHz frequencies are not used in the sea ice concentration algorithms. For simplicity, the channels are sometimes denoted as simply 19H, 19V, 22V, 37H, and 37V.

Beginning with the launch of F16 in 2003, the SSM/I sensor was replaced by the SSMIS sensor. The SSMIS sensor has the same 19.4, 22.2, and 37.0 GHz channels; however, the 85.5 GHz channels on SSM/I are replaced with 91.0 GHz channels on SSMIS. The SSMIS sensor also includes several higher frequency sounding channels that are not used for the sea ice products and are not archived at NSIDC. Depending on the platform, the satellites altitudes are 830 to 860 km and sensor (earth incidence) angles are 52.8 to 53.4 degrees. See Table 1 for details of each platform.

Parameter	Nimbus-7	DMSP-F8	DMSP-F11	DMSP-F13	DMSP-F17	DMSP-F18
Nominal Altitude (km)*	955	860	830	850	855	833
Inclination Angle (degrees)	99.1	98.8	98.8	98.8	98.8	98.6
Orbital Period (minutes)	104	102	101	102	102	102
Ascending Node Equatorial Crossing (approximate local time)	12:00 P.M.	6:00 A.M.	5:00 P.M.	5:43 P.M.	5:31 P.M.	8:00 P.M.
Algorithm Frequencies (GHz)*	18.0, 37.0	19.4, 37.0	19.4, 37.0	19.4, 37.0	19.4, 37.0	19.4, 37.0

Earth Incidence Angle (degrees)*	50.2	53.1	52.8	53.4	53.1	53.1

Table 1: Comparison of Nimbus and DMSP orbital parameters

*Indicates sensor and spacecraft orbital characteristics of the three sensors used in generating the sea ice concentrations.

A polar orbit and wide swath provides near-complete coverage at least once per day in the polar regions except for a small region around the North Pole called the pole hole. The SSMIS sensor has a wider swath width (1700 km) compared to the SSM/I sensor (1400 km), which reduces the size of the pole hole. The footprint or instantaneous field of view (IFOV) of the sensor varies with frequency (Table 2).

Frequency (GHz)	**SSM/I Footprint (km)**	**SSMIS Footprint (km)**
19.35	70 x 45	73 x 45
22.235	60 x 40	73 x 45
37.0	38 x 30	41 x 31
85.5/91.0	16 x 14	13 x 16

Table 2: IFOV of SSM/I and SSMIS frequencies

Regardless of footprint size, the low frequency channels (19.4 – 37.0 GHz) are gridded to a 25 km polar stereographic grid.

3. Algorithm Description

3.1 Algorithm Overview

The Sea Ice Concentration CDR algorithm uses concentration estimates derived at NSIDC from the NASA Team (Cavalieri et al., 1984) and Bootstrap (Comiso, 1986) algorithms as input data and merges them into a combined single concentration estimate based on the known characteristics of the two algorithms. First, the Bootstrap 10% concentration threshold is used as a cutoff to define the limit of the ice edge. Second, within the ice edge, the higher of the two concentration estimates from the NASA Team and Bootstrap algorithms is used for the CDR input value. The reason for these two approaches is discussed further in section 3.4.1.4. Automated quality control measures are implemented independently on the NASA Team and Bootstrap outputs. Two weather filters, based on ratios of channels sensitive to enhanced emission over open water, are used to filter weather effects. Separate land-spillover corrections are used for each of the algorithms to filter out much of the error due to mixed land/ocean grid cells. Finally, climatological ocean masks are applied to screen out errant retrievals of ice in regions where sea ice never occurs.

To remove spurious ice caused by residual weather effects and land spillover in passive microwave data, a number of quality control filters are applied to the resulting sea ice concentrations. First, two weather filters, based on ratios of channels sensitive to enhanced emission over open water, are used to remove spurious weather effects. Next, land-spillover corrections are used for each of the algorithms to remove much of the error due to mixed land/ocean grid cells. After applying these automated filters, a final climatological mask is applied to remove any remaining ice from regions where sea ice would not be possible. For the Northern Hemisphere, the masks used are the Polar Stereographic Valid Ice Masks Derived from National Ice Center Monthly Sea Ice Climatologies, available from NSIDC (https://nsidc.org/data/nsidc-0622). These masks do not have a Southern Hemisphere component. Therefore, for the Southern Hemisphere, climatological ocean masks, based on monthly average sea surface temperatures, are applied to screen out errant retrievals of ice in regions where sea ice never occurs.

3.2 Processing Outline

The following flow diagrams (Figure 1 and 2) describe the general processing for the finalized daily and monthly TCDR sea ice concentrations and the near-real-time provisional daily and monthly ICDR sea ice concentrations, respectively.

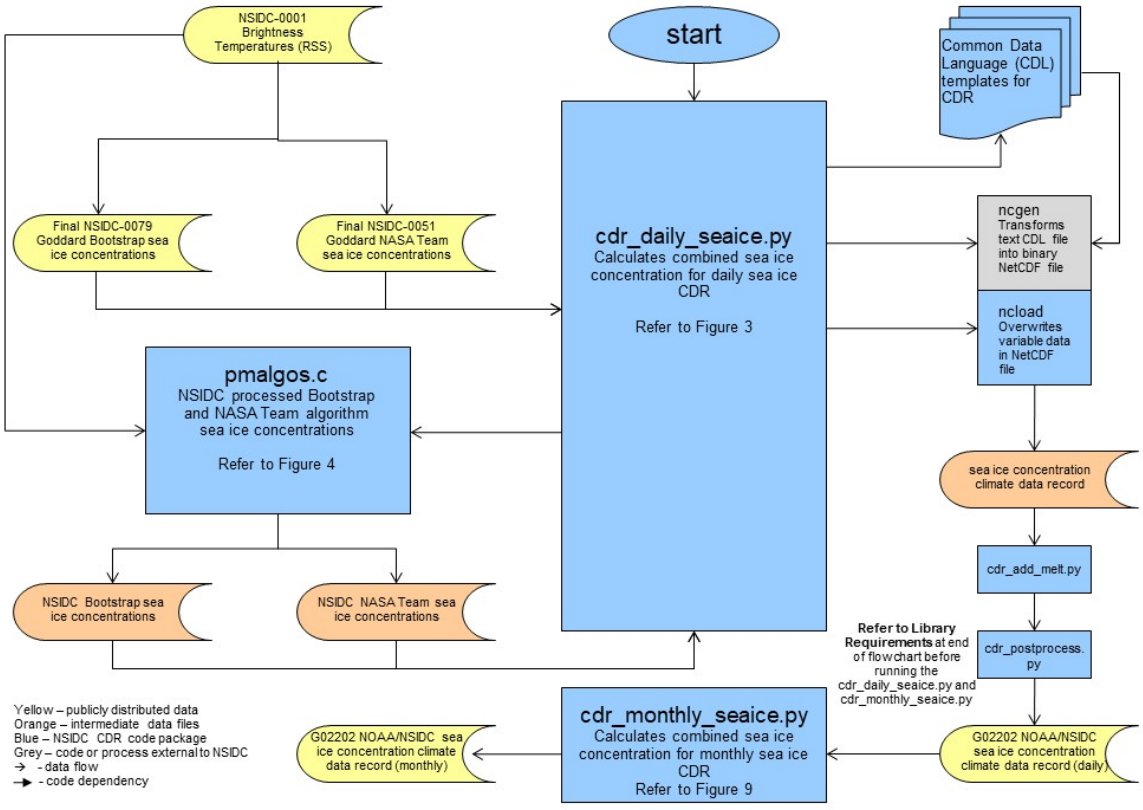

Figure 1: Finalized sea ice concentration TCDR processing overview

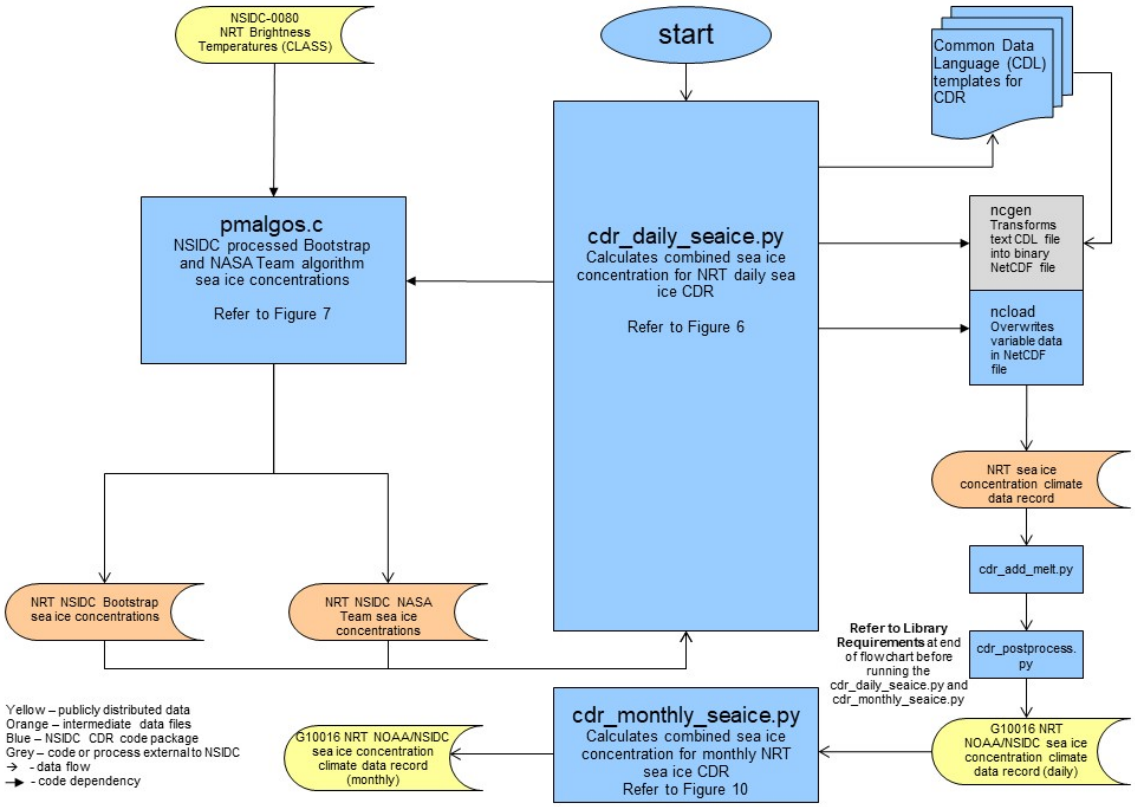

Figure 2: Near-Real-Time sea ice concentration ICDR processing overview

3.2.1 Daily Processing

The flow diagrams in Figures 3, 4, and 5 describe the processing of the daily finalized TCDR sea ice concentration in detail. The flow diagrams in Figures 6, 7, and 8 describe the processing of the daily near-real-time ICDR sea ice concentration in detail.

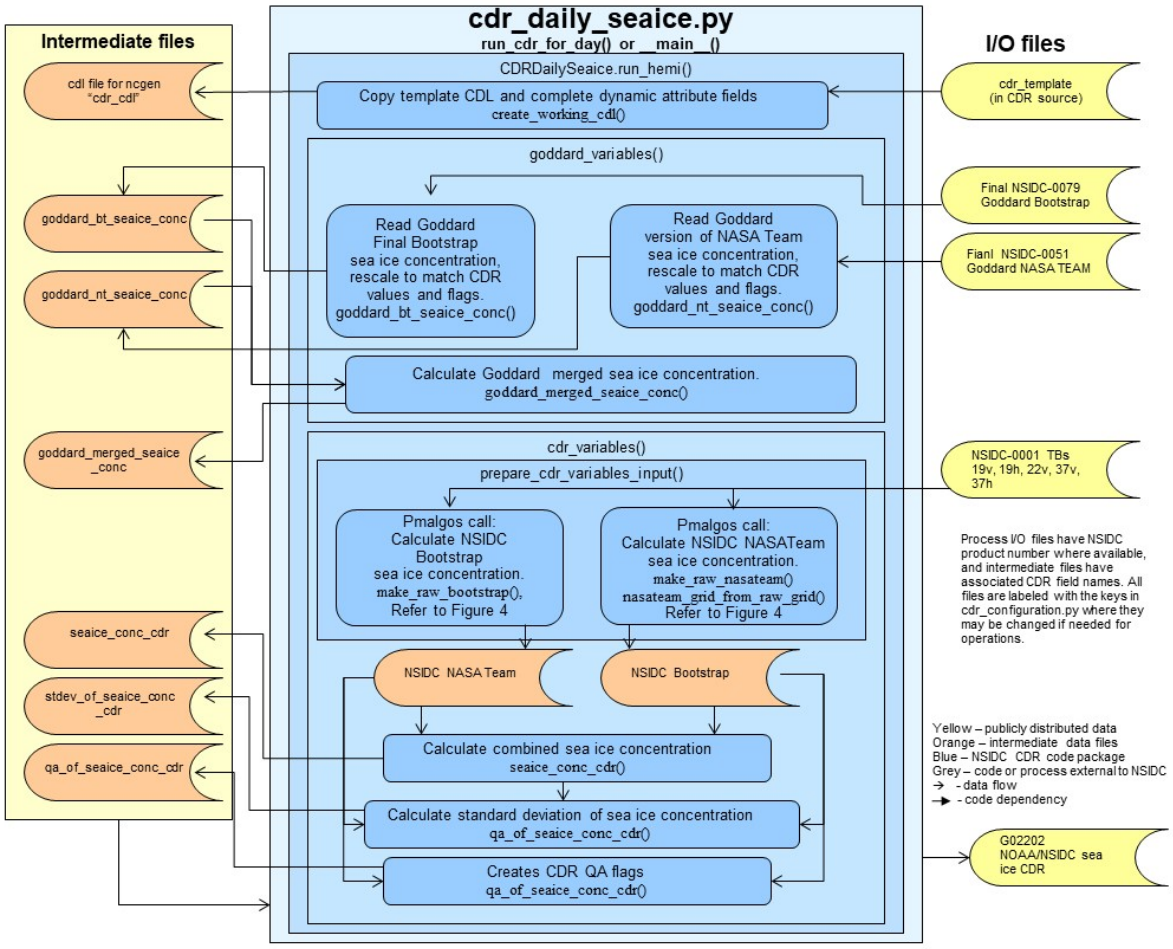

Figure 3: Overview of main python code for the daily finalized sea ice concentration TCDR processing

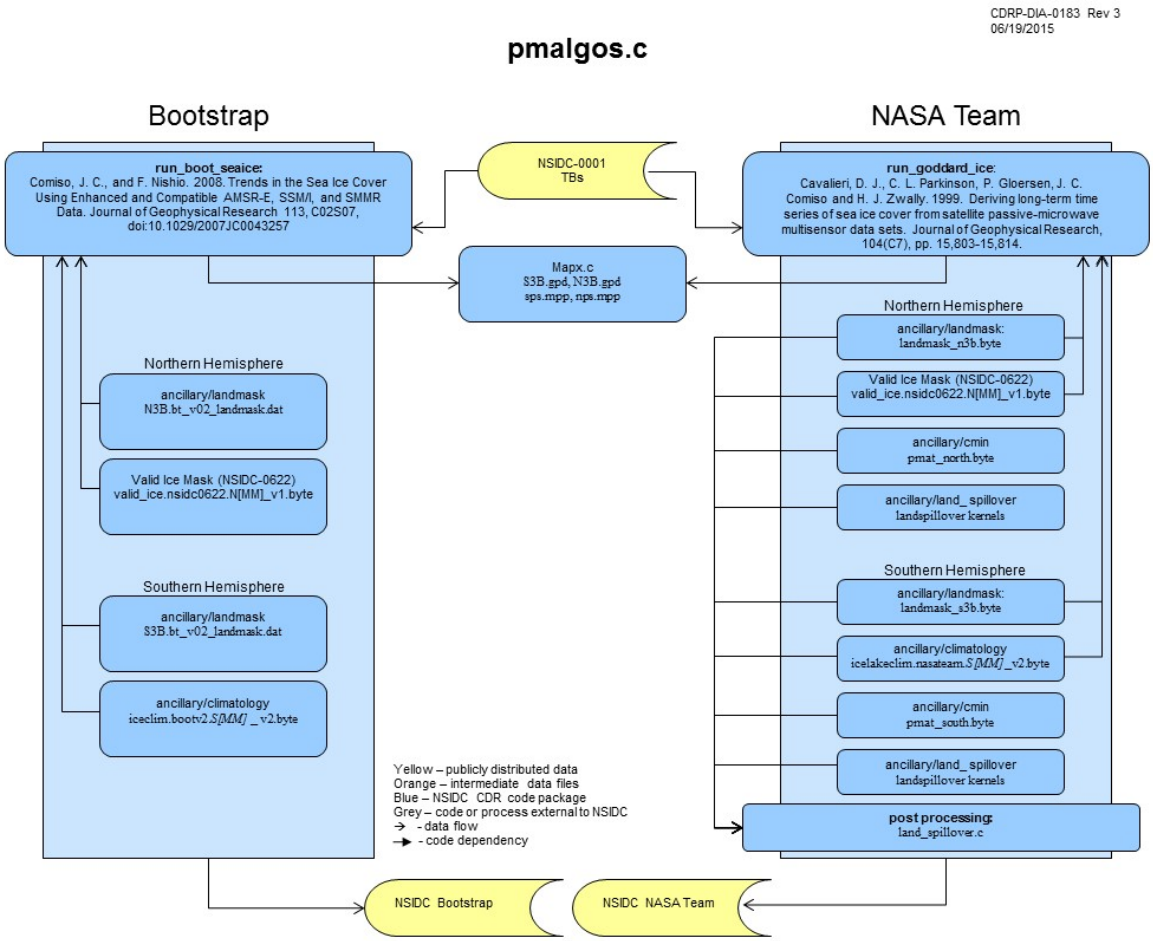

Figure 4: Overview of finalized Sea Ice Concentration TCDR algorithm C code

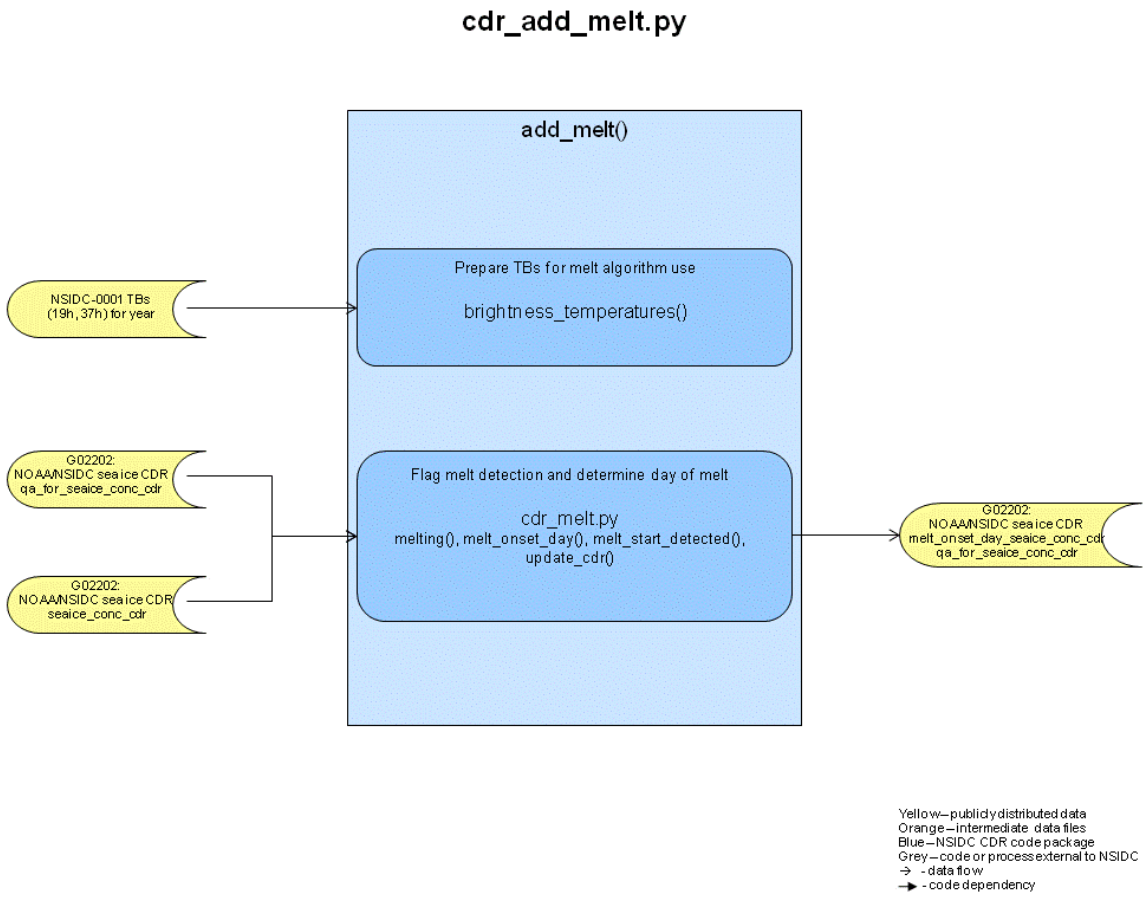

Figure 5: Overview of python code for adding melt start detection to finalized TCDR data

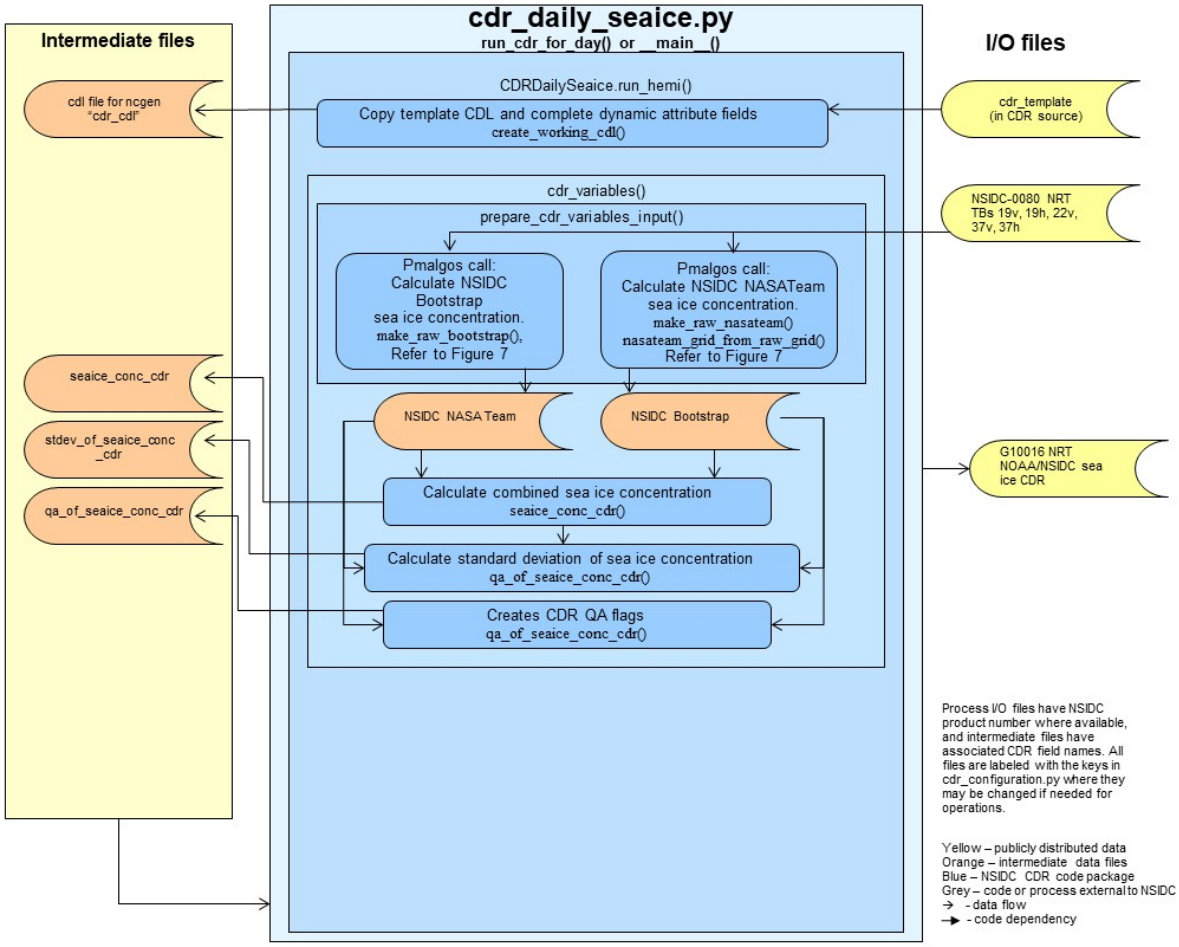

Figure 6: Overview of main python code for the daily near-real-time sea ice concentration ICDR processing

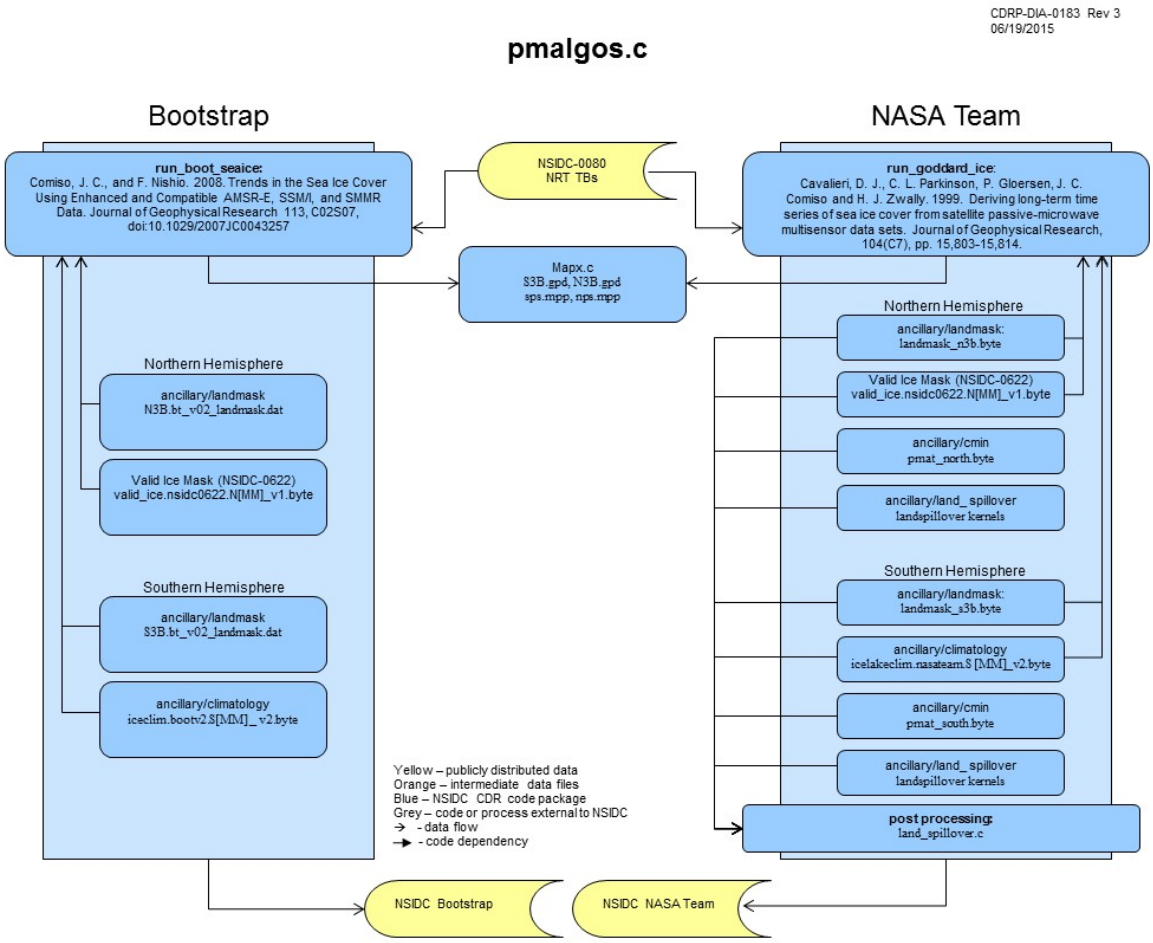

Figure 7: Overview of near-real-time sea ice concentration ICDR algorithm C code

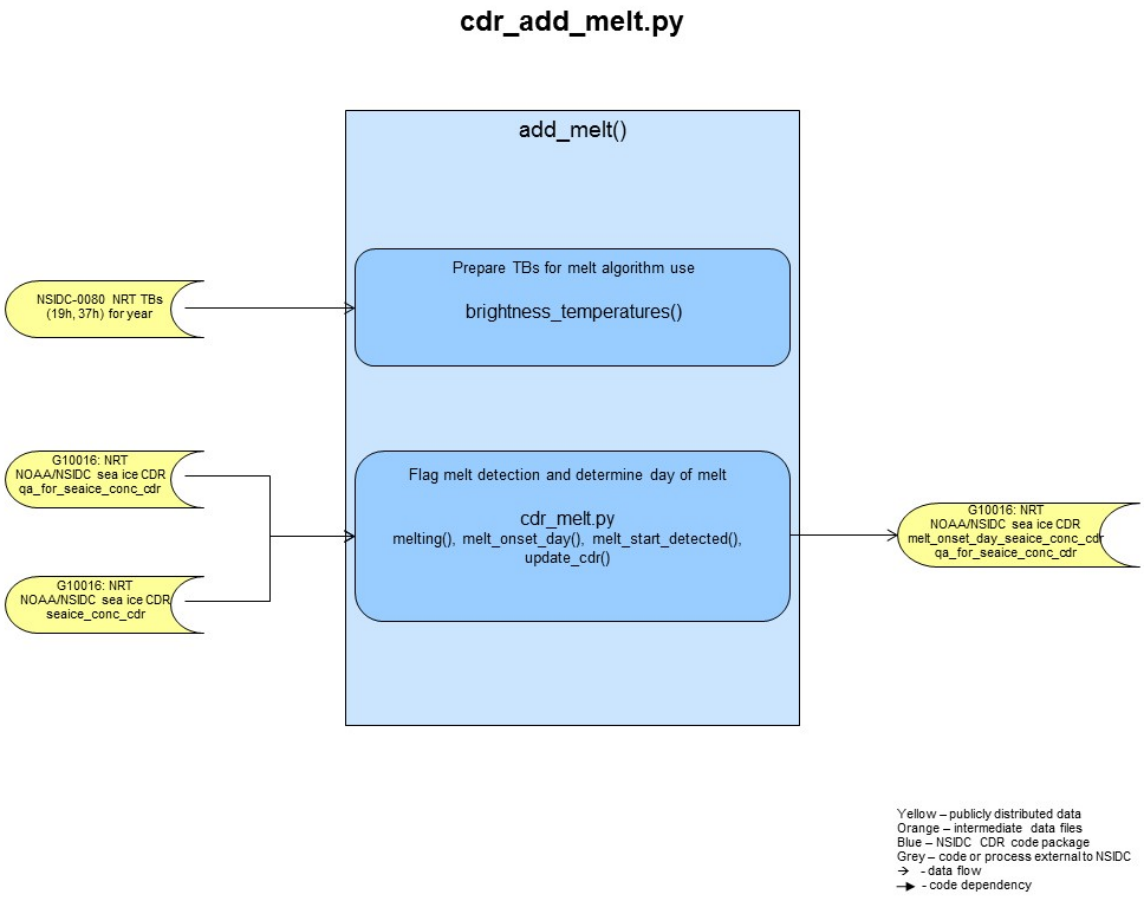

Figure 8: Overview of python code for adding melt start detection to near-real-time ICDR data

3.2.2 Monthly Processing

The flow diagrams in Figure 9 and Figure 10 describe the processing of the monthly CDR sea ice concentration for the finalized TCDR data and the near-real-time ICDR data, respectively.

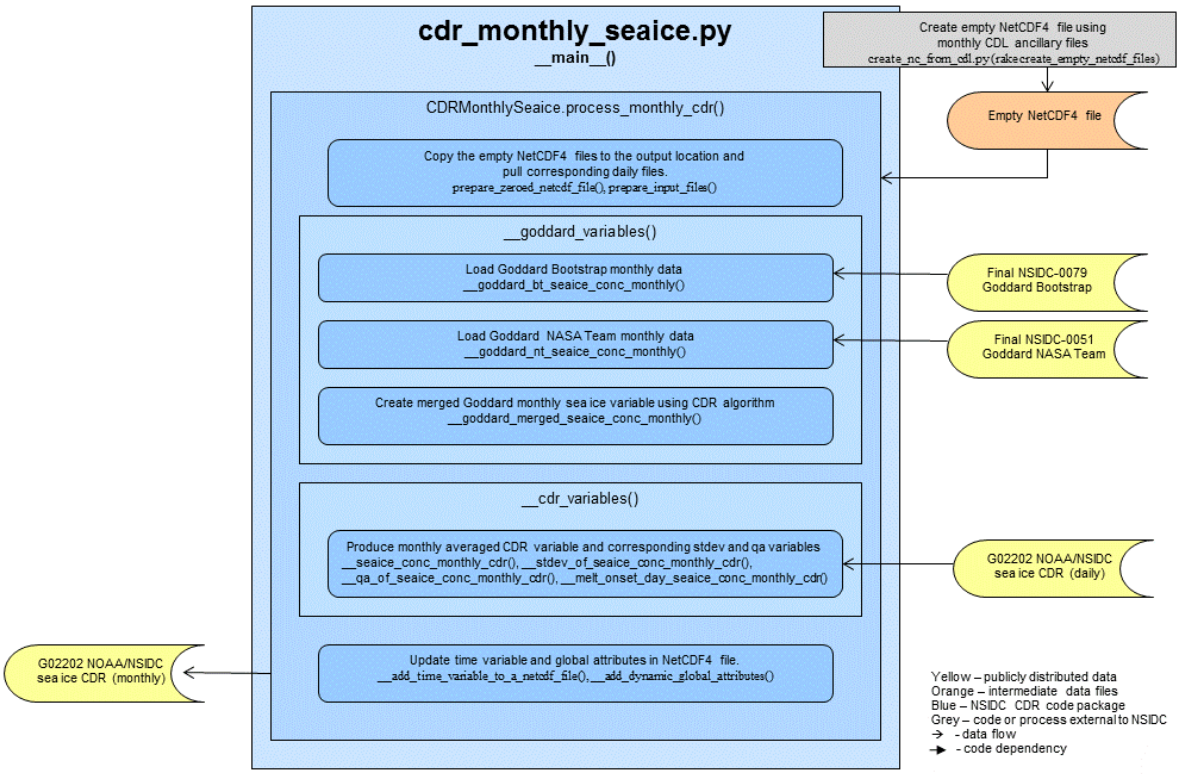

Figure 9: Monthly finalized TCDR processing

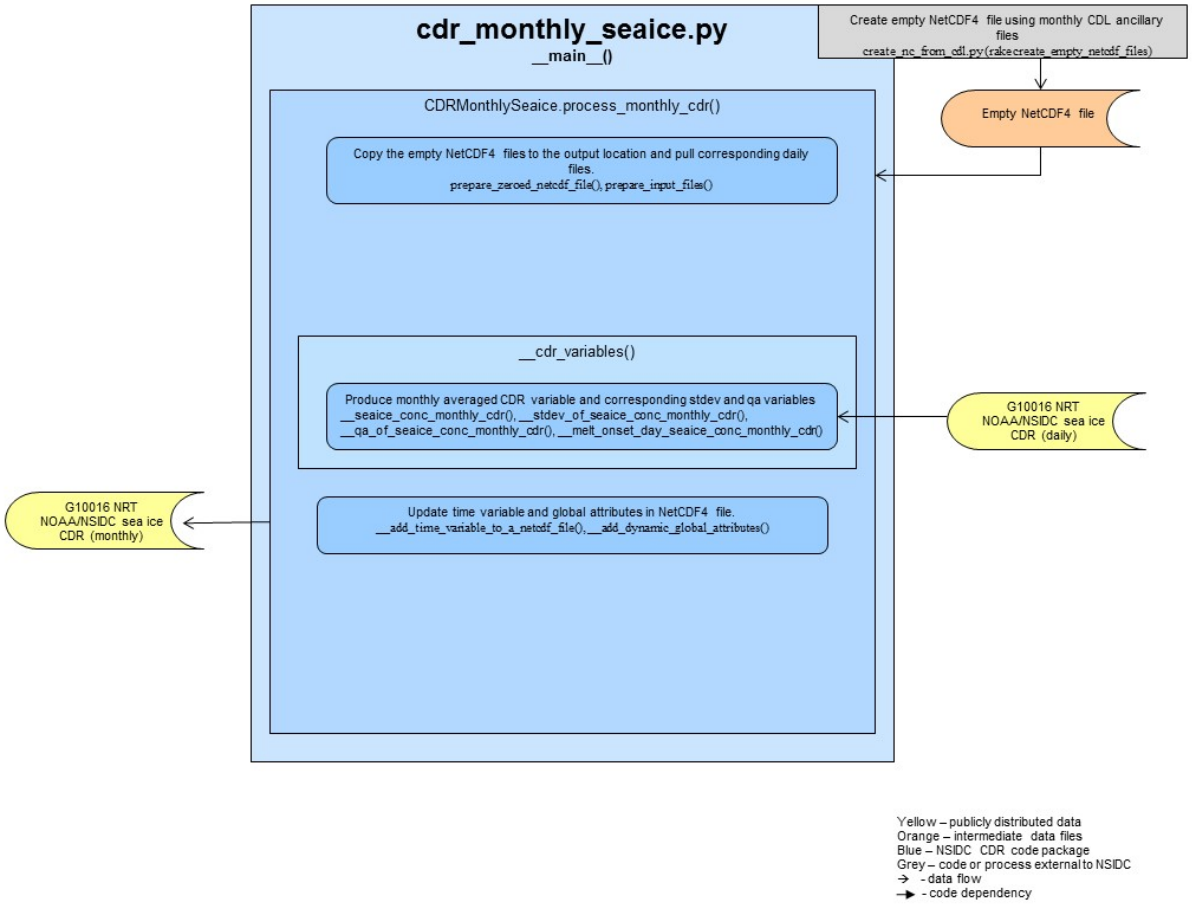

Figure 10: Monthly near-real-time ICDR processing

3.3 Algorithm Input

3.3.1 Primary Sensor Data

Calibrated and gridded brightness temperatures from SSM/I and SSMIS passive microwave sensors are used as the primary input data for this sea ice concentration CDR. These gridded brightness temperatures have a different source for the finalized TCDR and near-real-time ICDR portions of the product. For the TCDR data, these gridded brightness temperatures are produced from swath data obtained from RSS. For the ICDR data, these gridded brightness temperatures are produced from swath data obtained from NOAA CLASS. Both the RSS and CLASS brightness temperatures use enhanced processing methods to correct errors and improve calibration and geolocation. Specific processing information on the input swath data is available from RSS (http://www.ssmi.com/) and CLASS (https://www.class.ngdc.noaa.gov/release/data_available/dmsp/index.htm).

NSIDC puts both of the input swath data sets onto a 25 km polar stereographic grid for both Arctic and Antarctic regions. NSIDC also makes both of these input data products publicly available from their web site: DMSP SSM/I-SSMIS Daily Polar Gridded Brightness Temperatures data set (https://nsidc.org/data/nsidc-0001) for the TCDR and Near-Real-Time DMSP SSM/I-SSMIS Daily Polar Gridded Brightness Temperatures data set (https://nsidc.org/data/nsidc-0080) for the ICDR.

For current processing of the TCDR, NSIDC is using Version 7 RSS brightness temperatures. Earlier periods use different versions. Because the sea ice algorithms are intercalibrated at the product (concentration) level, the brightness temperature version is less important because the intercalibration adjustment includes any necessary changes due to differences in brightness temperature versions. However, when Version 7 is available for the entire DMSP record and resources allow, a full reprocessing will be considered. For the processing of the ICDR, NSIDC uses CLASS brightness temperatures that do not have a version number associated with them. These NRT data may contain errors and are not suitable for time series, anomalies, or trends analyses. Near-real-time products do not undergo quality assessment and are therefore not optimal for use in long-term climate studies. The near-real-time portion of this product are available from NSIDC as the Near-Real-Time NOAA/NSIDC Climate Data Record of Passive Microwave Sea Ice Concentration (https://nsidc.org/data/g10016). This NRT sea ice concentration ICDR is meant as a provisional interim estimate to span the gap before the availability of the finalized Sea Ice Concentration TCDR, which have an approximately one-year latency before they are available from NSDIC as the NOAA/NSIDC Climate Data Record of Passive Microwave Sea Ice Concentration (https://nsidc.org/data/g02202). However, once the RSS brightness temperatures become available, the finalized portion of the CDR is processed which replaces the near-real-time portion. Table 3 shows the instruments used for the input data for the CDR, and Table 4 and 5 show them for the Goddard-produced data.

Sensor	**Temporal Range**	**Source/Data Version**	**Product it Applies to**
DMSP-F18 SSMIS	Near-real-time	CLASS (no version given)	ICDR
DMSP-F17 SSMIS	01 Jan 2008 – most current processing date	RSS V7	TCDR
DMSP-F13 SSM/I	01 Oct 1995 – 31 Dec 2007	RSS V4	TCDR
DMSP-F11 SMM/I	03 Dec 1991 – 30 Sep 1995	RSS V3	TCDR
DMSP-F8 SSM/I	09 Jul 1987 – 02 Dec 1991 Note: There are no data from 3 December 1987 through 12 January 1988 due to satellite problems.	RSS V3	TCDR

Table 3: Version history and dates of the instruments used for the input brightness temperatures for the sea ice CDR variable.

Sensor	Temporal Range
DMSP-F17 SSMIS	01 Jan 2008 – most current processing date
DMSP-F13 SSM/I	30 Sep 1995 – 31 Dec 2007
DMSP-F11 SSM/I	19 Dec 1991 - 29 Sep 1995
DMSP-F8 SSM/I	21 Aug 1987 - 18 Dec 1991 Note: There are no data from 3 December 1987 through 12 January 1988 due to satellite problems.
Nimbus-7 SMMR	26 Oct 1978 - 20 Aug 1987

Table 4: Dates of the instruments used for the input brightness temperatures for the Goddard-produced NASA Team variables in the TCDR.

Sensor	Temporal Range
DMSP-F17 SSMIS	01 Jan 2008 – most current processing date
DMSP-F13 SSM/I	10 May 1995 – 31 Dec 2007
DMSP-F11 SSM/I	18 Dec 1991 - 09 May 1995
DMSP-F8 SSM/I	01 Aug 1987 - 17 Dec 1991 Note: There are no data from 3 December 1987 through 13 January 1988 due to satellite problems.
Nimbus-7 SMMR	01 Nov 1978 - 31 Jul 1987

Table 5. Dates of the instruments used for the input brightness temperatures for the Goddard-produced Bootstrap variables in the TCDR

The swath data are gridded onto a daily composite 25 km polar stereographic grid using a drop-in-the-bucket method. For each grid cell, all footprints from all passes each day whose centers fall within the grid cell are averaged together. Thus, some grid cells may be an average of several (4 or 5) passes during a given day and some may be from only one pass; some grid cells are typically not filled due to sensor characteristics, such as the large footprint. Note that the polar stereographic grid is not equal area; the latitude of true scale (tangent of the planar grid) is 70 degrees. The Northern Hemisphere grid is 304 columns by 448 rows, and the Southern Hemisphere grid is 316 columns by 332 rows. Further information on the polar stereographic grid used at NSIDC can be found on the NSIDC web site on the Polar Stereographic Projection and Grid web page (https://nsidc.org/data/polar_stereo/ps_grids.html).

The brightness temperatures are from SSM/I sensors on the DMSP-F8, -F11, and -F13 platforms as well as SSMIS data from the DMSP-F17 and -F18 platforms (Table 6). The rationale for using only these satellites was made to keep the equatorial crossing times as consistent as possible to minimize potential diurnal effects from data on sun-synchronous orbits of the DMSP satellites.

The passive microwave channels employed for the sea ice concentration product are the 19.4, 22.2, and 37.0 GHz frequencies. The NASA Team algorithm uses the 19.35 GHz horizontal (H) and vertical (V) polarization channels and the 37.0 GHz vertical

channel. The 22.2 GHz V channel is used with the 19.4 GHz V for one of the weather filters. The Bootstrap algorithm uses 37 GHz H and V channels and the 19.35 GHz V channel; it also uses the 22.2 GHz V channel for a weather filter.

Passive Microwave Sensor Sources for Sea Ice CDR						
Satellite	**Sensor**	**Frequencies (GHz)**	**Launch Date (Data Available) [Data at NSIDC]**	**Ascending Equatorial Crossing Time At Launch (Most Recent, Date)**	**Swath Width (km)**	**Mean Altitude (km)**
NIMBUS-7	SMMR*	6, 10, 18, 37	10/24/78 [10/25/78-8/20/87]	12:00	783	955
DMSP-F8	SSM/I	19, 22, 37, 85	6/18/87 [7/9/87-12/30/91]	06:15 (06:17, 9/2/95)	1400	840
DMSP-F11	SSM/I	19, 22, 37, 85	11/28/91 (12/6/91-5/16/00) [12/3/91-9/30/95]	18:11 (18:25, 9/2/95)	1400	859
DMSP-F13	SSM/I	19, 22, 37, 85	3/24/95 (3/25/95-11/19/09) [5/3/95-12/31/08]	17:42 (18:33, 11/28/07)	1400	850
DMSP-F17	SSMIS	19, 22, 37, 91+	11/4/06 (12/14/06-present) [1/1/07-3/31/16]]	(17:31, 11/28/07)	1700	850
DMSP-F18	SSMIS	19, 22, 37, 91+	10/18/09 (3/8/10-present) [4/1/16-present)	20:00	1700	833

Table 6: Brightness temperature sources for sea ice CDR. *SMMR is not included in the CDR parameter, but is employed by the Goddard-produced ancillary estimates. +SSMIS includes higher frequency channels not used in the sea ice CDR and not archived at NSIDC.

3.3.2 Ancillary Data

Ancillary data required for the product include: (A) a climatological minimum sea ice mask, CMIN, used for the NASA Team land-spillover correction, (B) ocean masks to define the limits of possible sea ice, (C) a melt onset estimate for the Northern Hemisphere to be used in the quality field, and (D) land masks imbedded within each field, based on masks developed by GSFC. Each of these is discussed further below.

A. Because of the large instantaneous field of view of the SSM/I and SSMIS sensors, mixed land-ocean grid cells occur. These present a problem for the automated concentration algorithm because the emission from the combined land-ocean region has a signature similar to sea ice and is interpreted as such by the algorithms. For the NASA Team algorithm, a filtering mechanism has been

implemented to automatically remove much of these false coastal ice grid cells by using a weighting based on the proximity of the grid cell to the coast and a minimum concentration matrix, CMIN. There is one CMIN field for each hemisphere. The CMIN matrix is described below in Section 3.4.1.3.

B. A near-real-time version of a snow melt onset over sea ice field algorithm by Drobot and Anderson (2001) is used as an input for the Northern Hemisphere quality indicator. Liquid water over the ice changes the surface emission resulting in errors in the algorithms, typically an underestimation of concentration. Thus, occurrence of melt in a grid cell is an indication of lower quality. This melt onset algorithm employs the same gridded brightness temperatures from RSS.

C. Each sea ice concentration and associated fields include an imbedded land mask. Grid cells are defined as land, coast (land adjacent to ocean), inland lake, or ocean. Both the NASA Team and Bootstrap algorithms use the same mask in the Northern Hemisphere, which can be found on NSIDC's Masks and Overlays web page (https://nsidc.org/data/polar_stereo/tools_masks.html#land_masks). In the Southern Hemisphere, the Bootstrap algorithm uses an updated mask reflecting changes in the coastline due to ice-shelf movement. For consistency through the CDR time series in the Southern Hemisphere, the CDR field is considered land if either the input NASA Team or Bootstrap fields is considered land.

D. Ocean climatology masks are used to remove any remaining spurious ice not filtered by automated corrections (discussed in 3.4.1.3) in regions where sea ice is not possible. There are monthly masks for each hemisphere. For the Southern Hemisphere, the source and application of these masks are described in Section 3.4.1.3. These masks can be obtained from NSIDC at: https://nsidc.org/data/pm/ocean-masks. For the Northern Hemisphere, remaining spurious ice is removed using the Polar Stereographic Valid Ice Masks Derived from National Ice Center Monthly Sea Ice Climatologies. There are 12 masks, one for each month. They are available from NSIDC (https://nsidc.org/data/nsidc-0622).

3.3.3 Derived Data

Not applicable.

3.3.4 Forward Models

Not applicable.

3.4 Theoretical Description

Passive microwave radiation is naturally emitted by the Earth's surface and overlying atmosphere. This emission is a complex function of the microwave radiative properties of the emitting body (Hallikainen and Winebrenner, 1992). However, for the purposes of microwave remote sensing, the relationship can be described as a simple function of the physical temperature (T) of the emitting body and the emissivity (ε) of the body.

$$T_B = \varepsilon * T \qquad (6)$$

T_B is the brightness temperature and is the parameter (after calibrations) retrieved by satellite sensors and is the input parameter to passive microwave sea ice concentration algorithms.

3.4.1 Physical and Mathematical Description

The microwave electromagnetic properties of sea ice are a function of the physical properties of the ice, such as crystal structure, salinity, temperature, or snow cover. In addition, open water typically has an electromagnetic emission signature that is distinct from sea ice emission (Eppler et al., 1992). These properties form the basis for passive microwave retrieval of sea ice concentrations.

Specifically, the unfrozen water surface is highly reflective in much of the microwave regime, resulting in low emission (Figure 5). In addition, emission from liquid water is highly polarized. When salt water initially freezes into first-year (FY) ice (ice that has formed since the end of the previous melt season), the microwave emission changes substantially; the surface emission increases and is only weakly polarized. Over time as freezing continues, brine pockets within the sea ice drain, particularly if the sea ice survives a summer melt season when much of the brine is flushed by melt water. This multi-year (MY) ice has a more complex signature with characteristics generally between water and FY ice. Other surface features can modify the microwave emission, particularly snow cover, which can scatter the ice surface emission and/or emit radiation from within the snow pack. Atmospheric emission also contributes to any signal received by a satellite sensor. These issues result in uncertainties in the retrieved concentrations, which are discussed further below.

Because of the complexities of the sea ice surface as well as surface and atmospheric emission and scattering, direct physical relationships between the microwave emission and the physical sea ice concentration are not feasible. Thus, the standard approach is to derive concentration through empirical relationships. These empirically-derived algorithms take advantage of the fact that brightness temperature in microwave frequencies tend to cluster around consistent values for pure surface types (100% water or 100% sea ice). Concentration can then be derived using a simple linear mixing equation (Zwally et al., 1983) for any brightness temperature that falls between the two pure surface values:

$$T_B = T_I C_I + T_O(1-C_I) \quad (7)$$

Where T_B is the observed brightness temperature, T_I is the brightness temperature for 100% sea ice, T_O is the brightness temperature for open water, and C_I is the sea ice concentration.

In reality, such an approach is limited by the surface ambiguities and atmospheric emission. Using combinations of more than one frequency and polarization limits these effects, resulting in better discrimination between water and different ice types and a more accurate concentration estimate.

There have been numerous algorithms derived using various combinations of the frequencies and polarizations on the SMMR and SSM/I sensors. Two commonly used algorithms are the NASA Team (Cavalieri et al., 1984) and Bootstrap (Comiso, 1986), both developed at NASA GSFC. The sea ice concentration CDR described here is produced via a combination of estimates from the NASA Team algorithm and the Bootstrap algorithm. Below, each algorithm is described in more detail followed by a description of quality control (QC) procedures and the procedure to merge the two algorithm estimates into the final CDR product.

3.4.1.1 NASA Team Algorithm

The NASA Team algorithm uses brightness temperatures from the 19V, 19H, and 37V channels. The methodology is based on two brightness temperature ratios, the polarization ratio (PR) and spectral gradient ratio (GR), as defined below:

$$PR(19) = [T_B(19V) - T_B(19H))]/[T_B(19V) + T_B(19H)] \quad (8)$$

$$GR(37V/19V) = [T_B(37V) - T_B(19V)]/[T_B(37V) + T_B(19V)] \quad (9)$$

When PR and GR are plotted against each other, brightness temperature values tend to cluster in two locations, an open water (0% ice) point and a line representing 100% ice concentration, roughly forming a triangle. The concentration of a grid cell with a given GR and PR value is calculated by a linear interpolation between the open water point and the 100% line segment (Figure 5).

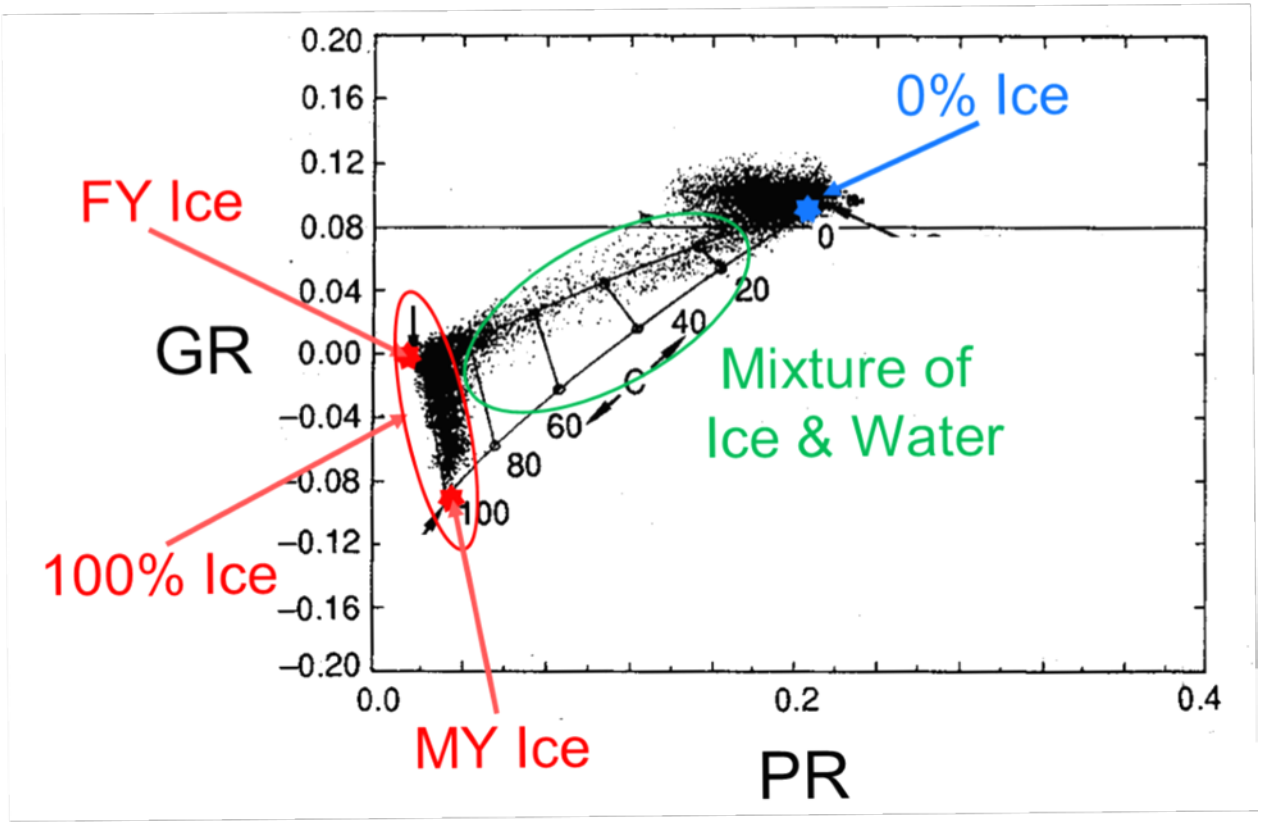

Figure 11: Sample plot of GR vs. PR with typical clustering of grid cell values (small dots) around the 0% ice (open water) point (blue star) and the 100% ice line (circled in red). First year (FY) ice clusters at the top of the 100% ice line, and multi-year (MY) ice clusters at the bottom. Points with a mixture of ice and water (circled in green) fall between these two extremes. Adapted from Figure 10-2 of Steffen et al. (1992).

Mathematically, these two ratios are combined in the following two equations:

$$C_F = (a_0 + a_1PR + a_2GR + a_3PR * GR)/D \quad (10)$$

$$C_M = (b_0 + b_1PR + b_2GR + b_3PR * GR)/D \quad (11)$$

$$where\ D = c_0 + c_1PR + c_2GR + c_3PR * GR \quad (12)$$

The C_F and C_M parameters represent ice concentration for two different sea ice types. In the Arctic, these generally correspond to FY ice (C_F: ice that has grown since the previous summer) and MY ice (C_M: ice that has survived at least one melt season). In the Antarctic, due to its small amount of MY ice and different ice characteristics, C_M and C_F do not necessarily correspond to the age types and are simply denoted as Type A and Type B. Total ice concentration (C_T) is the sum of the two partial concentrations.

$$C_T = C_F + C_M \quad (13)$$

The a_i, b_i, c_i (i=0, 3) coefficients are empirically derived from nine observed T_Bs at each of the 3 channels for 3 pure surface types (two sea ice and one open water). These T_Bs, called tie-points, were originally derived for the SMMR sensor (Cavalieri et al., 1984). The tie-points were adjusted for subsequent sensors via intercalibration of the concentration/extent fields during sensor overlap periods to ensure consistency through the time series (Cavalieri et al., 1999). Tie-point adjustments are made via a linear regression analysis along with additional adjustments for open water tie-points. The tie-point adjustment procedure and tie-point values for all sensors through F13 SSM/I are provided in Cavalieri et al. (1999). Tie-points for F17 are described in Cavalieri et al. (2011).

NIMBUS 7 SMMR				
Arctic		**18H**	**18V**	**37V**
	OW	98.5	168.7	199.4
	FY	225.2	242.2	239.8
	MY	186.8	210.2	180.8
Antarctic				
	OW	98.5	168.7	199.4
	A	232.2	247.1	245.5
	B	205.2	237.0	210.0
DMSP-F8 SSMI				
Arctic		**19H þ**	**19V þ**	**37V þ**
	OW	113.2 +0.2	183.4 +0.5	204.0 -1.6
	FY	235.5	251.5	242.0
	MY	198.5	222.1	184.2
Antarctic				
	OW	117.0 +7.7	185.3 +3.8	207.1 +5.3
	A	242.6	256.6	248.1
	B	215.7	246.9	212.4
DMSP-F11 SSMI				
Arctic		**19H þ**	**19V þ**	**37V þ**
	OW	113.6 +0.5	185.1 +0.5	204.8 +0.2
	FY	235.3	251.4	242.0
	MY	198.3	222.5	185.1
Antarctic				
	OW	115.7 +0.1	186.2 -0.4	207.1 -1.4
	A	241.2	255.5	245.6
	B	214.6	246.2	211.3 -2.0
DMSP-F13 SSMI				

Arctic		**19H**	**19V**	**37V**
	OW	114.4	185.2	205.2
	FY	235.4	251.2	241.1
	MY	198.6	222.4	186.2
Antarctic				
	OW	117.0 +0.3	186.0	206.9
	A	241.4	256.0	245.6
	B	214.9	246.6	211.1
DMSP-F17 SSMIS				
Arctic		**19H**	**19V**	**37V**
	OW	113.4	184.9	207.1
	FY	232.0	248.4	242.3
	MY	196.0	220.7	188.5
Antarctic				
	OW	113.4	184.9	207.1
	A	237.8	253.1	246.6
	B	211.9	244.4	212.6
DMSP-F18 SSMIS				
Arctic		**19H**	**19V**	**37V**
	OW	113.4	184.9	207.1
	FY	232.0	248.4	242.3
	MY	196.0	220.7	188.5
Antarctic				
	OW	113.4	184.9	207.1
	A	237.8	253.1	246.6
	B	211.9	244.4	212.6

Table 7: Tie-point values (in Kelvin) for each SSM/I and SSMIS sensor along with original SMMR values. The þ column is the additional adjustment required for open water tie-points (no adjustment was needed for F17 or F18).

The algorithm can sometimes obtain concentration values that are less than 0% or are greater 100%, both of which are clearly unphysical. Such values are set to 0% and 100%, respectively.

3.4.1.2 Bootstrap Algorithm

Like the NASA Team algorithm, the Bootstrap algorithm is empirically derived based on relationships of brightness temperatures at different channels. The Bootstrap method

uses the fact that scatter plots of different sets of channels show distinct clusters that correspond to pure surface types (100% sea ice or open water).

Figure 12 shows a schematic of the general relationship between two channels. Points that fall along line segment AD represent 100% ice cover. Points that cluster around point O represent open water (0% ice). Concentration for a point B is determined by a linear interpolation along the distance from O to I where I is the intersection of segment OB and segment AD. This is described by the following equation:

$$C = (T_B - T_O)/(T_I - T_O) \qquad (14)$$

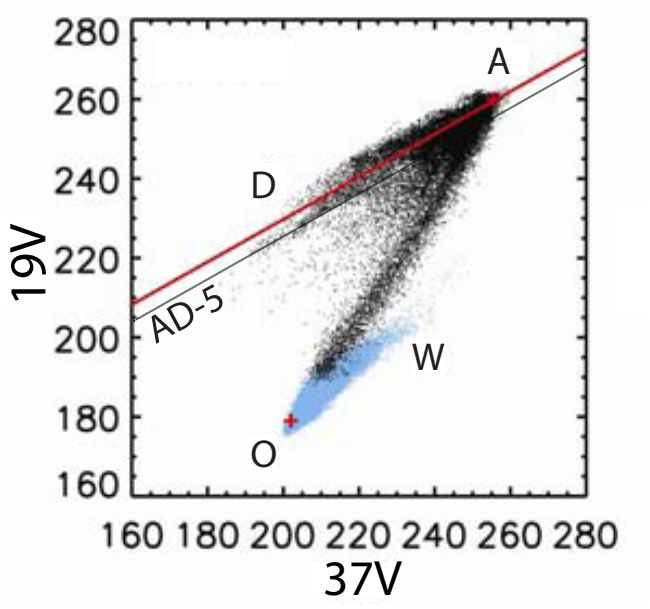

Figure 12: Example of the relationship of the 19V vs. 37V T_B (in Kelvin) used in the Bootstrap algorithm. Brightness temperatures typically cluster around the line segments AD (representing 100% sea ice) and OW (representing 100% open water). For points that fall below the AD-5 line (dotted line), bootstrap uses T_B relationships for 37H vs. 37V. Adapted from Comiso and Nishio (2008).

The Bootstrap algorithm uses two such combinations, 37H versus 37V and 19V versus 37V, denoted as HV37 and V1937, respectively. Points that fall within 5 K of the AD segment in a HV37 plot, corresponding roughly to concentrations > 90%, use this approach. Points that fall below the AD-5 line, use the V1937 relationship to derive the concentration. Slope and offset values for line segment AD were originally derived for each hemisphere for different seasonal conditions (Table 2 in Comiso et al, 1997). However, a newer formulation, employed in this CDR, was developed where slope and offsets are derived for each daily field based on the clustering within the daily brightness temperatures (Comiso and Nishio, 2008).

Intersensor calibration is done similar to the way it is done for the NASA Team algorithm where brightness temperatures from the sensors are regressed against each other. One sensor's brightness temperatures are adjusted based on the regression with the other sensor. However, because the slope and offset values are derived each day based on the brightness temperatures, there are not specific slope/offset (tie-point) adjustments between sensors. Also, while the NASA Team originally derived the tie-points for SMMR and then adjusted future sensors to maintain consistency with SMMR, the newest version of the Bootstrap algorithm used AMSR-E as a baseline and adjusted SSM/I and SMMR brightness temperatures to be consistent with AMSR-E. Because AMSR-E is a newer and more advanced sensor, the intersensor calibration should be more accurate and more consistent overall. This is discussed further in Comiso and Nishio (2008).

The algorithm can sometimes obtain concentration values that are less than 0% or are greater 100%, both of which are clearly unphysical. Such values are set to 0% and 100% respectively.

3.4.1.3 Quality Control Procedures

Several automated quality control procedures have been implemented to filter out spurious concentration values. The main sources of these spurious ice grid cells are: ocean surface brightness temperature variation, atmospheric emission, and mixed land-ocean IFOV in a grid cell. These are first discussed in general and then the specific filters used to remove much of these effects are described for each of the NASA Team and Bootstrap products.

Both algorithms assume that open water can be represented as a single point in the clustering of different channel combinations. However, it is evident in Figures 11 and 12 above that there is considerable spread around the open water point. This is primarily due to weather effects, namely: roughening of the ocean surface by winds, which increases the microwave emission of the water, and atmospheric emission, primarily due to water vapor and liquid water (clouds), which will also increase the emission retrieved by the sensor. Atmospheric emission is most pronounced during rain fall over the open ocean. Emission from the atmosphere has the largest effect on the 19.35 GHz channels because they are near to frequencies (22.235 GHz) in which there is strong water vapor emission.

Spurious ice is also common along ice-free coasts. Because of the large IFOV (up to 73 km x 45 km for 19.35 GHz), brightness temperature values from ocean grid cells near the coast often contain microwave emission from both land and ocean. These mixed grid cells of ocean/land have a brightness temperature signature that is often interpreted by the algorithms as sea ice. When sea ice is actually present along the coast, the effect is small, but when there is no ice present, artifacts of false ice appear. This is commonly called the land-spillover effect because emission from the land surface "spills over" into ocean grid cells.

Automated filters used to correct these spurious concentrations are discussed below. It is possible, however, that the automated filters may also remove real ice in some conditions.

NASA Team Weather Filters

Spurious ice over open water is removed by a threshold of the GR3719 ratio (Equation 9) and an additional GR2219 ratio:

$$GR(22V/19V) = [T_B(22V) - T_B(19V)]/[T_B(22V) + T_B(19V)] \quad (15)$$

Using the following criteria:

$$GR3719 > 0.050 \rightarrow concentration = 0 \quad (16)$$

$$GR2219 > 0.045 \rightarrow concentration = 0 \quad (17)$$

This applies to all conditions except for F17 SSMIS in the Southern Hemisphere, where a slightly different GR3719 threshold is used:

$$GR3719(SH, F17) > 0.053 \rightarrow concentration = 0 \quad (18)$$

Bootstrap Weather Filters

The Bootstrap algorithm also uses combinations of 19V, 22V, and 37V as a weather filter, but the methodology follows the overall Bootstrap by thresholding above a cluster of points in (1) 19V vs. 37V, and (2) 19V vs. (22V-19V) T_B scatter plots (Figure 13).

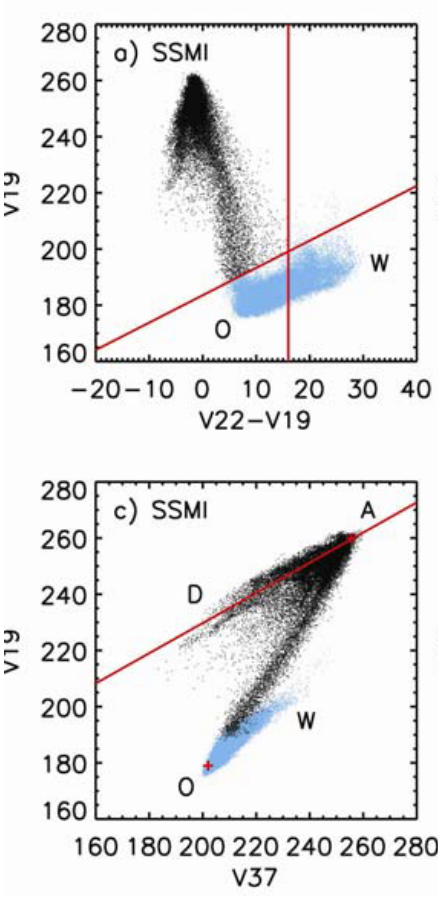

Figure 13: Sample scatter plot of 19V vs. (22V-19V) (top) and 19V vs. 37V (bottom) T_Bs. Values shaded in blue around the OW segment are masked to 0% concentration. From Comiso and Nishio (2008).

NASA Team Land-Spillover Correction

For the NASA Team algorithm, a filtering mechanism has been implemented to automatically remove many of the false coastal ice grid cells by using a weighting based on the proximity of the grid cell to the coast and a minimum concentration matrix, CMIN. This method removes many, but not all errors due to land-spillover. The procedure is done in three steps (summarized from Cavalieri et al., 1999):

1. A static matrix, M, was created for each hemisphere's polar stereographic grid. Using the land mask, all grid cells were defined as shore, near-shore, off-shore, or non-coastal ocean. A shore cell is one that is directly adjacent to land. For example, for grid cell (I,J) in Figure 14, at least one A grid cell is land. A near-shore grid cell is one grid cell removed from land; in Figure 14, no A grid cells are land, but at least one B cell is land. An off-shore grid is two grid cells removed from land, that is no A or B cells are land, but at least one C cell is land. Off-shore grid cells are more than three grid cells from land, so no A, B, or C cells around a point (I,J) are land. The rationale for this is that any influence will

decrease farther from shore; and with a maximum footprint scale of 70 km (19.35 GHz SSM/I channels are 70 x 45 km), any land effect should not extend more than three 25 km grid cells from land.

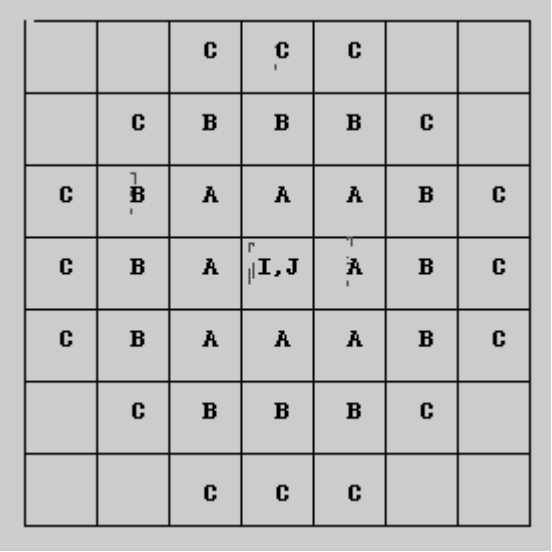

Figure 14: Example of grid cell neighbor to define coastal proximity classification for a grid cell, (I,J). From Cavalieri et al. (1999).

2. A minimum ice concentration field, CMIN, is created from one year of data: 1992. First, a matrix of minimum monthly average concentrations is created for the year. Then these concentrations are adjusted based on the classifications in the M matrix. At off-shore grid cells, any CMIN values exceeding 20% are reduced to 20%. At near-shore grid cells, any CMIN values exceeding 40% are reduced to 40%. At shore grid cells, any CMIN values exceeding 60% are reduced to 60%.
3. During processing, concentrations in the offshore, near-shore, and shore grid cells are adjusted using the CMIN matrix. For each grid cell class in CMIN, a “neighborhood” is defined. For off-shore cells, the neighborhood is the 3 x 3 box surrounding the cell. A near-shore cell neighborhood is a 5 x 5 box, and a shore neighborhood is a 7 x 7 box. For each neighborhood box, if at least 3 grid cells contain open water (<15% ice), then the concentration of the center grid cell is adjusted by subtracting the concentration of the coincident grid cell in the CMIN matrix. Wherever the calculation results in negative values, the concentration is set to 0%.

Bootstrap Land-Spillover Correction

The Bootstrap algorithm uses a simpler method developed by Cho et al. (1996). It uses a 3 x 3 filter around each grid cell. If at least one of the 3 x 3 group of grid cells is land then the center grid value is replaced by the minimum non-land value within the 3 x 3 grid cell group.

Removing False Ice

Weather effects can cause the passive microwave signature of seawater to appear like that of ice (Cavalieri 1995). Atmospheric water vapor is often the reason behind false-ice detection. Most of these false-ice signatures are removed with a standard brightness-temperature filter, but some are too close to those of real ice and require another method to be removed. While the automatic weather-filter thresholds remove most false ice over open water, there are times when extreme weather conditions (heavy rain, strong winds) still result in false ice, often in regions where sea ice is not physically possible. This includes false ice along the coast far from ice-covered regions that is not removed by the land-spillover correction (discussed above in the NASA Team Land-Spillover Correction and the Bootstrap Land-Spillover Correction sections). Thus, a final QC correction is applied to the NASA Team and Bootstrap estimates.

Ocean Climatology Masks for Southern Hemisphere

Thus, in the Southern Hemisphere, masks based on the monthly sea surface temperature (SST) climatology of Levitus and Boyer (1994) are used. A temperature threshold of 275 K was used to determine the mask boundary for each month. Any sea ice concentrations above 15% calculated by the algorithms in regions where the masks do not allow sea ice are set to zero in the final concentration estimates. These masks can be obtained from NSIDC at: https://nsidc.org/data/pm/ocean-masks.

Valid Ice Masks for Northern Hemisphere

The best way to evaluate where ice can be is to look at a climatology of sea ice occurrence, where the climatology is built from Arctic-wide sea ice analyses over as long a period as possible from many different sources. These show where ice detected by the satellite data algorithm is most likely to be valid ice, based on where ice has existed in the past.

For the Northern Hemisphere, these weather effects and land spillovers are corrected with the Polar Stereographic Valid Ice Masks Derived from National Ice Center Monthly Sea Ice Climatologies, available from NSIDC (https://nsidc.org/data/nsidc-0622). The climatology used for these masks is the National Ice Center Arctic Sea Ice Charts and Climatologies in Gridded Format. It includes 12 masks showing the maximum sea ice extent, one for each month of the year, over the period 1972 to 2007.

For the NASA Team ancillary variables in the TCDR, NASA GSFC applies the SST mask to the Northern Hemisphere, using a threshold of 278 K. However, for automated processing, this was found to be insufficient because of the large numbers of weather effects within the mask region. Thus, the valid ice mask was deemed more suitable for the automated CDR product.

3.4.1.4 Sea Ice Concentration Climate Data Record Algorithm

NSIDC processes the input brightness temperatures into two different intermediate sea ice concentrations using two Goddard-developed algorithms: NASA Team (Cavalieri et al., 1984) and Bootstrap (Comiso, 1986).

The processing for the NASA Team component of the Sea Ice concentration CDR is nearly the same as the Goddard processing with two known differences. First, NSIDC uses a new brightness temperature version for the F8 period from what Goddard processed. Second, NSIDC uses a corrected version of brightness temperatures for F11 and F13, while Goddard used the uncorrected version. Spatial and temporal interpolation is done by Goddard, and they also perform an additional manual QC step. In comparisons between the two, there are occasional small variances due to the differences noted here.

Goddard processed their sea ice concentrations using the NSIDC gridded brightness temperature version available at the time of processing. For the TCDR, NSIDC is using the currently available version distributed by NSIDC (https://nsidc.org/data/nsidc-0001). See Table 3 for a list of the versions and the time periods these were used.

For F11 and F13, after initial processing of brightness temperatures at NSIDC and NASA Team concentrations at Goddard, small errors were discovered in the brightness temperature processing resulting in the inclusion of some bad scan lines. These bad scan lines resulted in some small artifacts in the gridded Goddard concentration estimates. After discovery of the brightness temperature processing error, NSIDC reprocessed the affected F11 and F13 data, but Goddard did not re-run their concentrations.

For missing grid cells, Goddard employed a spatial or temporal interpolation to fill in the missing values. For isolated missing grid cells, a spatial average from surrounding non-missing grid cells is used to fill the missing grid cell. For larger areas of missing data, due to missing swaths of brightness temperature data or bad data removed by the manual QC described below, a temporal interpolation is used where concentration estimates from the day before and the day after are averaged to fill the missing region.

The most significant difference between the processing at NSIDC and at Goddard is the use of a manual inspection to correct grid cells with erroneous concentration values. Each daily field was examined at Goddard and a hand-cleaning process was used to remove any sea ice grid cells that were deemed to be erroneous. The majority of these erroneous sea ice values were false coastal ice that were not removed by the land-spillover correction, and false ice over the ocean that were not removed by either weather filter or the ocean mask. In these cases, the grid cell is simply replaced with a 0% value. In very rare cases, some legitimate sea ice grid cells were deemed to have clearly incorrect concentration values. These concentration values were removed and the affected grid cells were considered missing. These missing values were then filled via the interpolation discussed above.

The NASA Team and Bootstrap algorithms and their associated automated QC procedures are run independently. Then, the algorithm concentration values are combined to create the CDR concentration field by selecting the larger concentration value between the NASA Team and Bootstrap outputs for each grid cell and implementing a 10% concentration threshold based on Bootstrap concentrations. The details and rationale for these two steps are provided below:

1. At each sea ice grid cell, the concentration between the NASA Team and the Bootstrap output are compared, and whichever value is greater is selected as the CDR value. Both algorithms tend to underestimate concentration, as is discussed more in section 5.5, but the source and the effect on the underestimation differs between algorithms. The NASA Team algorithm, because it uses a ratio of brightness temperatures, tends to cancel out any physical temperature effects. The Bootstrap algorithm uses relationships between two brightness temperatures that are dependent on physical temperature. Thus, physical temperature changes can affect Bootstrap estimates. This occurs primarily in regimes with very low temperatures: winter in the high Arctic and near the Antarctic coast (Comiso et al., 1997). During winter conditions with more moderate temperatures, NASA Team concentrations also tend to have more of a low bias (Kwok, 2002; Meier, 2005). During melt conditions, both algorithms tend to underestimate concentration; but the effect is more pronounced in the NASA Team algorithm. Also, the NASA Team estimates are biased lower than the Bootstrap estimates (Comiso et al., 1997; Meier, 2005; Andersen et. al, 2007).

   While these characteristics of the algorithm are true in an overall general sense, ice conditions and algorithm performance can vary from grid cell to grid cell; and in some cases, this approach will result in an overestimation of concentration (Meier, 2005). However, using the higher concentration between the two algorithms will tend to reduce the overall underestimation of the CDR estimate.

2. A 10% concentration threshold based on the Bootstrap concentration is used to define the ice edge (the boundary between ice and open water). A 15% cutoff is a common standard that has been in use for many years (Zwally et al., 1983) and in comparison studies with other satellite data, has agreed well, on an average basis, with the observed ice edge (Cavalieri et al., 1991; Meier et al., 2003). Also, the applied weather filters typically remove most concentrations below 15% (Cavalier et al., 1999). However, there are indications that the Bootstrap algorithm can potentially detect ice at as low as 8% levels (Comiso and Nishio, 2008). Thus a 10% cutoff is used within the CDR data fields. However, the validity of this assumption depends on the character of the ice edge as well as ocean and atmospheric conditions and for total extent and area calculations a 15% cutoff is still recommended. The 10% cutoff in the CDR field will miss some real ice, but low concentrations have much higher uncertainties and because of the large footprint of the SSM/I and SSMIS sensors (70 km x 45 km and 73 km x 45 km for 19.35 GHz, respectively) any ice edge has precision of two or three 25

km x 25 km grid cells. The 10% cutoff removes many potentially high error concentration estimates and provides a standard throughout the time series.

The rationale for using the Bootstrap estimates only to define the edge is two-fold. First, just the maximum value criteria between Bootstrap and NASA Team discussed will yield more low-concentration, high-error grid cells than using only one algorithm. Second, the Bootstrap data have been recently reprocessed (Comiso and Nishio, 2008) to intercalibrate ice extents with AMSR-E Bootstrap products. The AMSR-E sensor has a much smaller footprint and, thus, is able to obtain a more precise ice edge (Comiso and Nishio, 2008). So, the SSM/I-SSMIS Bootstrap algorithm likely yields extent and area fields that better match the real values. Another possible approach is to require that both the NASA Team and Bootstrap estimates must have concentrations greater than 15% to be included, but it is felt that this would be too stringent and miss some legitimate sea ice grid cells. Also, such a combination could possibly introduce small artifacts to trends in long-term sea ice extent time series.

3. A final issue needs to be addressed for the Southern Hemisphere. In this region, the NASA Team and Bootstrap algorithms use different land masks. The Bootstrap algorithm uses a newer mask that takes into account recent changes in the ice shelves, particularly Larson-B along the Antarctic Peninsula (Scambos et al., 2004). The updated mask allows concentrations to be obtained in the newly open regions. However, such a mask introduces an inconsistency into the time series because more sea ice is detected, not because of change in climatic conditions, but because an area opened up that would have already been sea ice covered were it not for the ice shelf presence. For the sea ice concentration CDR field, a combined land mask is used where a grid cell that is land in either the NASA Team or Bootstrap algorithm is flagged as land in the CDR. This is overly conservative and yields more land than either of the individual NASA Team and Bootstrap masks, but is consistent throughout the time series. Users wishing to study specific regions in and near the changing ice shelves can use the Goddard NASA Team or Bootstrap concentrations included in the product as ancillary fields discussed further in section 3.4.4.

3.4.2 Data Merging Strategy

Both the NASA Team and Bootstrap algorithms employ varying tie-points to account for changes in sensors and spacecraft. These tie-point adjustments are derived from regressions of brightness temperatures during overlap periods. The adjustments are made at the product level by adjusting the algorithm coefficients so that the derived sea ice fields are as consistent as possible. This approach was found to be more successful than intercalibrating the input brightness temperature fields. The reasons for this are due to several factors. First, the products are derived on daily mean gridded brightness temperatures using a simple drop-in-the-bucket average. A new sensor on a new sun-synchronous satellite will have a different equatorial crossing time. This means that the gridded brightness temperature for a given grid cell will be comprised of swath

brightness temperature values from different times of day between data from the old sensor versus the new sensor. Because sea ice, as well as the overlying atmosphere, varies over time, this will result in inconsistencies in the brightness temperature signal even when the brightness temperatures themselves are fully intercalibrated. Second, the sea ice varies on scales far smaller than the footprint of the passive microwave sensors. Thus, any retrieved brightness temperature is likely a mixture of several different surfaces (for example, first-year vs. multi-year, smooth vs. rough/ridged, deep snow vs. snow free, etc.). This makes it difficult to directly match up brightness temperatures from different sensors to the same sea ice conditions over which to intercalibrate. Finally, transitions between sensors may result in a change of frequency, notably for SMMR and SSM/I, where the 18.7 GHz frequency on SMMR was replaced by a 19.35 GHz frequency on SSM/I.

The NASA Team approach uses sensor-specific hemispheric tie-points for each transition (Cavalieri et al., 1999; Cavalieri et al., 2011). Tie-points were originally derived for the SMMR sensor and subsequent transitions to SSM/I and SSMIS adjusted the tie-points to be consistent with the original SMMR record. The Bootstrap algorithm uses daily varying hemispheric tie-points, derived via linear regression analysis on clusters of brightness temperature values of the relevant channels, as in Figure 12 (Comiso, 2009), and the adjustment involves a linear regression between brightness temperatures (Comiso and Nishio, 2008). Also, in contrast to the NASA Team, Bootstrap tie-points for SMMR and SSM/I are derived from matching fields from the AMSR-E sensor, which is newer and more accurate.

3.4.3 Look-Up Table Description

There are a considerable number of external static data grids and masks used to create this product. This section lists and describes these grids and their origins arranged in alphabetical order by directory and then file name.

3.4.3.1 Pole Hole Mask

The pole hole mask file contains a mask to create a consistent area of missing data at the North Pole where the satellites cannot take measurements. They were created from the data within the nsidc-0051 data set (https://nsidc.org/data/nsidc-0051) provided to NSIDC by the GSFC.

The files are named the following:

```
ROOT/ancillary/
       gsfc_pole_hole.NPP
```

Where PP is the platform identifier (*07*, *13*, or *17*). The gsfc_pole_hole.N07 file corresponds to Nimbus 7 and is used for the SMMR data. The gsfc_pole_hole.N13 file is used for the F08, F11, and F13 data because the size of the pole holes is the same for all three platforms, and the gsfc_pole_hole_N17 file is used for F17 and F18 data.

3.4.3.2 Sea Surface Temperature Files

These 12 sea surface temperature climatology files (Levitus and Boyer, 1994) are used as input to Southern Hemisphere Bootstrap processing.

The files are named the following:

```
ROOT/ancillary/bootstrap_seaice/
       sst_s_MM.hdf
```

Where *s* is the Southern Hemisphere and *MM* is the two digit month (*01 - 12*).

3.4.3.3 Bootstrap Climatology Masks

These files are Northern and Southern Hemisphere 1/0 masks used in Bootstrap algorithm processing in the CDR code. The value 1 represents places where ice could possibly occur.

The files are named the following:

```
ROOT/ancillary/climatology/
       icelim.bootv2.NMM_v1.byte
       icelim.bootv2.SMM_v2.byte
```

Where *MM* is the two digit month (*01 – 12*).

3.4.3.4 NASA Team Climatology Masks

These files are Southern hemisphere 1/0 masks used in NASA Team algorithm processing in the CDR code. The value 1 represents places where ice might possibly occur.

The files are named the following:

```
ROOT/ancillary/climatology/
       icelakeclim.nasateam.SMM_v2.byte
```

Where *MM* is the two digit month.

3.4.3.5 Spillover Correction Matrices

These files represent the input P-matrix data used to compute the weights in the spillover correction and were provided by Nicolo DiGirolamo at GSFC in Greenbelt, MD. They are described in the Cavalieri et. al. (1999). These files were chosen to most accurately reproduce the pre-existing NSIDC sea ice concentration data sets as they are currently in use at GSFC.

The files are named the following:

```
ROOT/ancillary/cmin/
```

```
        pmat_north.byte
        pmat_south.byte
```

3.4.3.6 Bootstrap Land/Coast/Ocean Masks

These files are the Northern and Southern bootstrap land/coast/ocean masks. The Northern hemisphere mask was created from the data in NSIDC-0051 (https://nsidc.org/data/nsidc-0051). Because the Southern hemisphere data for the bootstrap algorithm has a different land shape than NASA team, this mask was created by an expansion operation of the ocean data onto the land data from NSIDC-0079 (https://nsidc.org/data/nsidc-0079) and taking that intersection as coast.

The files are named the following:

```
ROOT/ancillary/landmask/
        N3B.bootstrap_v02.landmask.dat
        S3B.bootstrap_v02.landmask.dat
```

3.4.3.7 CDR Land/Coast/Shore Masks

These files are the Northern and Southern Hemisphere masks used for the combined layers of the CDR product. The Northern Hemisphere mask was created using the existing mask from NSIDC-0051 (https://nsidc.org/data/nsidc-0051) and using kernel operations to compute shore and near-shore values. The Southern hemisphere mask was created using an intersection of the land values from NSIDC-0051 and NSIDC-0079 (https://nsidc.org/data/nsidc-0079). After this intersection was computed, a coast value was determined by the expansion of the ocean data atop the land data and using this intersection as coast. Additionally, because the region of Tierra Del Fuego is the same in the NSIDC-0051 and NSIDC-0079 products, the land/coast/ocean mask around this region was copied from NSIDC-0051. After computing the land/coast/ocean areas of the Southern Hemisphere, the same kernel operations were used to compute shore and near-shore data. The values are provided in Table 8.

Value	Description
0	Open water
1	N/A
2	Coast
3	Land
4	Lake
5	Shore (1 grid cell from land)
6	Near-shore (2 grid cells from land)

Table 8: CDR land/coast/shore mask values.

The files are named the following:

```
ROOT/ancillary/landmask/
       landCoastShoreMask.north.bin
       landCoastShoreMask.south.bin
```

3.4.3.8 NASA Team Land/Ocean Masks

These files are the Northern and Southern Hemisphere 1/0 masks of land/ocean computed from the NSIDC-0051 data product. These files are used in the CDR processing of the NASA Team sea ice.

The files are named the following:

```
ROOT/ancillary/landmask/
       landmask-n3b.byte
       landmask-s3b.byte
```

3.4.3.9 Northern Hemisphere Valid Ice Masks

These files are the masks for the Northern Hemisphere that remove spurious ice caused by residual weather effects and land spillover in passive microwave data. For a description of how these were created see the Polar Stereographic Valid Ice Masks Derived from National Ice Center Monthly Sea Ice Climatologies web page (https://nsidc.org/data/nsidc-0622).

The files are named the following:

```
ROOT/ancillary/climatology/
       valid_ice.nsidc0622.N[MM]_v1.byte
```

Where *MM* is the 2-digit month abbreviation and the range of years describes the years of data put into the computations.

3.4.3.10 Southern Hemisphere Climatology Masks

This is the climatology file used for the Southern Hemisphere. These were computed using the monthly climatological sea surface temperatures data from the NOAA Ocean Atlas (Levitus and Boyer, 1994). (3.4.3.2)

These data were converted to a mask to correct for residual weather effects according to NASA Technical Memorandum 104647 (https://nsidc.org/data/pm/nsidc0051-gsfc-seaice).

The file is named the following:

```
ROOT/ancillary/oceanmask/
       oceanmask.SMM_v2.bin
```

Where MM is the two-digit month.

3.4.4 Algorithm Output

The sea ice CDR code creates daily and monthly NetCDF data files. Each daily and monthly CDR file contains four primary CDR fields: a CDR concentration estimate, a standard deviation field, a melt onset flag, and a quality assessment field. In addition, for the finalized sea ice TCDR only, three ancillary concentration fields based on the individual NASA Team and Bootstrap fields processed by NASA Goddard are also included. Each field is a byte array (except for the standard deviation field that is a float array) on the polar stereographic grid: 304 columns by 448 rows (136,192 bytes) for the Northern Hemisphere and 316 columns by 332 rows (104,912 bytes) for the Southern Hemisphere. In the two sub-sections below, the daily and the monthly fields are described in detail.

3.4.4.1 Fields in the daily CDR files

The TCDR and ICDR both contain sea ice concentration, standard deviation, melt onset, and quality assessment fields, but the TCDR contains an extra three ancillary fields:

1. seaice_conc_cdr
2. stdev_for_seaice_conc_cdr
3. melt_onset_day_seaice_conc_cdr
4. qa_of_seaice_conc_cdr
5. goddard_nt_seaice_conc (TCDR only)
6. goddard_bt_seaice_conc (TCDR only)
7. goddard_merged_seaice_conc (TCDR only)

These CDR fields are explained below:

1. Sea Ice Concentration CDR

   This field, named seaice_conc_cdr, contains the sea ice concentration values for the CDR, scaled from 0-100%. This field (and the standard deviation and QA fields discussed below) is processed entirely at NSIDC with all processing steps fully documented (Section 3.4.1.4). For the TCDR, it includes the entire SSM/I-SSMIS time series, 1987-most recent process. For the ICDR, it includes SSMIS for all NRT data. The flag values for the sea ice concentration variables are given in Table 9.

Flag Name	Value
Land	254
Coast/land adjacent to Ocean	253
Missing	255
Lakes	252
Northern Hemisphere pole hole (the	251

region around the pole not imaged by the sensor)	

Table 9: Sea ice concentration variables flag values

2. Spatial Standard Deviation of Sea Ice Concentration

This field, named stdev_for_seaice_conc_cdr, contains the standard deviation of both the NASA Team and Bootstrap concentration estimate at each ocean/sea ice grid cell for that grid cell and the surrounding 8 grid cells (Figure 15). The standard deviation is calculated from the total of two 3 x 3 arrays of grid cells (one of NASA Team concentrations and one of Bootstrap concentrations), for 18 grid cells in total. Land grid cells within the 3 x 3 array are not included in the calculation; thus, along the coast, fewer than 18 values are used. Any missing grid cells (for example, the pole hole in the Northern Hemisphere) are also not included in the standard deviation. A minimum of 6 valid concentration values out of the 18 total are required to compute a standard deviation. Thus, some grid cells within small bays and inlets may not have a standard deviation value; such cells are likely to be potentially affected by land-spillover and should be considered to have high uncertainties.

This field is meant to give an indication of the uncertainties in the daily CDR concentration estimate. It is not a quantitative error estimate and should not be used as such. However, it does provide a useful guide to users as to the relative accuracy of concentration estimates relative to surrounding grid cells and can be used to derive relative weights for comparisons, interpolations, or assimilation studies. In winter conditions, away from the ice edge or coast where spatial variability occurs, standard deviations are typically a few percent (Cavalieri et al., 1984) and can potentially serve as a quantitative upper limit of the concentration error (Gloersen et al., 1993).

The error sources for sea ice concentration are described in detail below, but high standard-deviation values will generally correspond to regions where concentration errors are likely higher.

First, isolated sea ice grid cells along the coastline that result from the land-spillover issue discussed above will have higher standard deviations compared to ice-free ocean or high concentration ice cover along the coast because of the mixture of ice and open water (0% ice) in the calculation.

Another region of higher errors occurs along the ice-water boundary (the ice edge) due to limitations in the sensor resolution, to motion of the ice during the 24-hour average period, and to melt/growth of ice. These high gradient regions will have high standard deviation values.

Finally, during melt, the surface and atmospheric effects become relatively larger, leading to more spatial variability and higher standard deviation values. The melt

also tends to cause the algorithms to underestimate concentration because they incorrectly interpret the surface melt on top of the ice as increased open water. The NASA Team concentrations generally have a large low bias compared to the Bootstrap concentrations. This is the rationale for computing the standard deviation from both of the algorithms instead of the combined CDR estimate or just one of the algorithms. The lower relative bias in the NASA Team during melt compared to Bootstrap will yield increased standard deviation values, better indicating the presence of melt than using only the CDR concentration standard deviation.

Standard deviation values range from 0-1, and the fill value is -1.

3. Day of Melt Onset

   This field, named melt_onset_day_seaice_conc_cdr, contains the day of year on which melting sea ice was first detected in each grid cell. Once detected, the value is retained for the rest of the year. For example, if a grid cell started melting on day 73, the variable for the grid cell on that day will be 73, as will all subsequent days until the end of the year. The melt onset day is only calculated for the melt season: days 60 through 244, inclusive. Before melting is detected or if no melt is ever detected for that grid cell, the value will be -1 (missing / fill value).

   The conditions for melt onset at a particular grid cell are the following:

   - Melt detected:
     - Concentration >= 50% at the beginning of the season
     - Grid cell is not land, coast, shore (1 grid cell from coast), near-shore (2 grid cells from coast), or lake
   - Current sea ice concentration >= 50%
   - Brightness temperature delta (19H - 37H) < 2K
   - Presence of brightness temperatures for both channels (19H, 37H)

   Note: To calculate the melt onset for F17 and F18 data, the input brightness temperatures are first scaled as follows:

$$19H\_scaled = 1.021 * 19H - 1.681 \quad (19)$$

$$37H\_scaled = 1.001 * 37H - 0.650 \quad (20)$$

   These equations were derived by a regression between F17 and F13 brightness temperatures during March through September 2007 when there was an overlap

period between the two satellites. Regressions were run for each daily average brightness temperature field and slope and intercept values were calculated. These daily slope and intercept values were then averaged over the entire March through September period to derive the equations above.

The reason for applying this adjustment is to account for differences between the F17 and F13 sensors, including sensor characteristics (sensor footprint, geometry), differences in orbit (time of equatorial crossing), etc. For the NASA Team sea ice concentration algorithm, the differences between the two sensors are accounted for by adjusting the algorithm tie-points (Cavalieri et al., 2011). For the Bootstrap sea ice concentration algorithm, only a regression is needed because tie-points are derived daily from the brightness temperature fields. For the melt onset, Equations 19 and 20 are used to make this adjustment.

4. Quality Assessment (QA) Flags

   This field, named qa_of_seaice_conc_cdr, provides additional assessment to complement the standard deviation field. This field includes flags for source (BT or NT) of concentration value, melt state, masked regions, and coastal ice outside of the pack ice that may be due to the land-spillover effect. See Table 10.

   Each CDR concentration grid cell uses the concentration from the highest value of the Bootstrap or NASA Team concentration value for that grid cell. A flag is designated in this field to denote which algorithm concentration value is used at each grid cell.

   One of the largest contributors to errors in concentration estimates occurs when surface melt begins (see section 5.5.2). Thus, a melt flag (melt_start_detected) is implemented in the Northern Hemisphere to indicate where melt may be occurring. The melt onset test is performed only in the Northern Hemisphere because the character of the ice cover in the Southern Hemisphere, typified by strong melt-refreeze cycles, does not yield a reliable melt threshold in passive microwave brightness temperature data (Willmes et al., 2009).

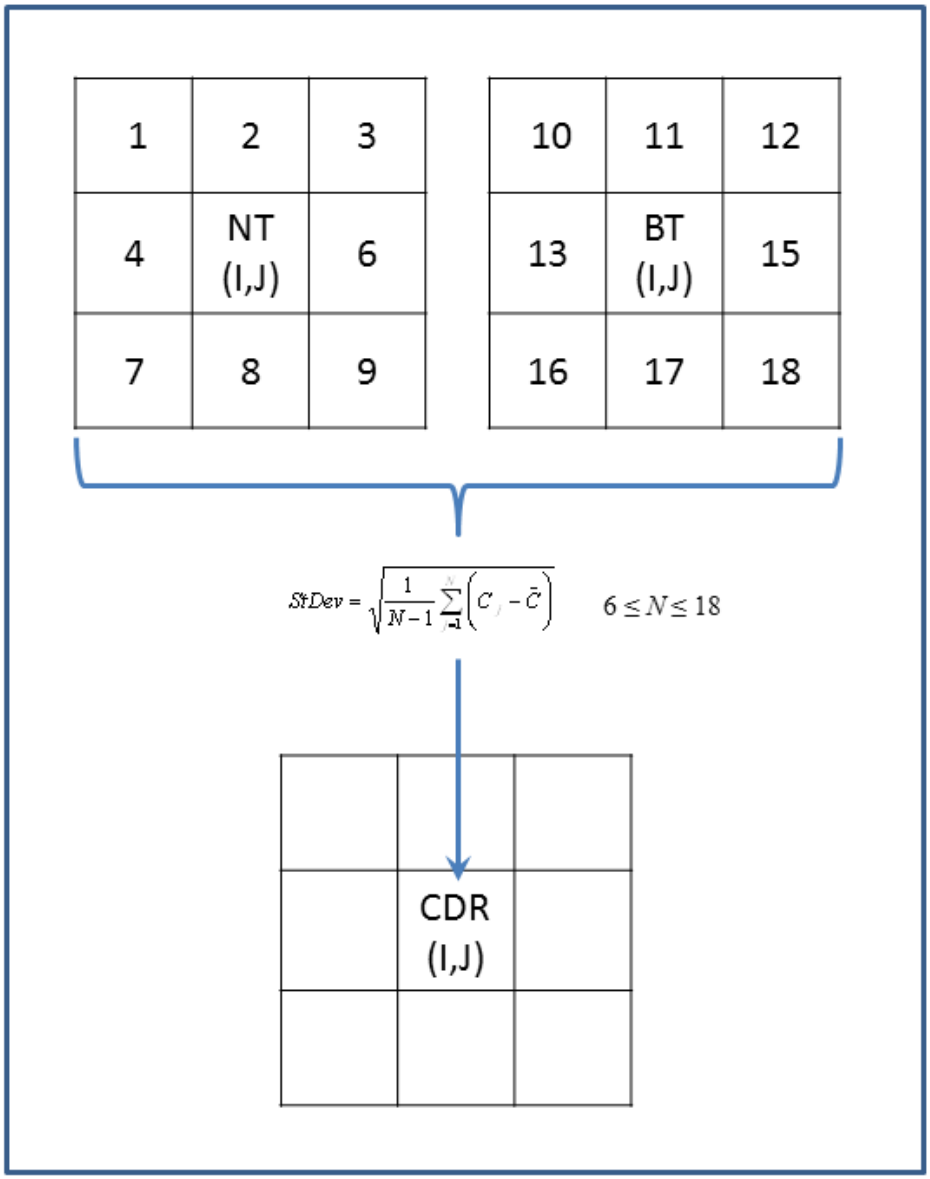

Figure 15: Schematic of grid cell values used in calculation of the CDR standard deviation field. All non-missing ocean/sea ice concentration values (C), from both the NASA Team and Bootstrap algorithm, of the 3 x 3 box surrounding each (I,J) grid cell (up to 18 total values) are used to calculate the standard deviation. A minimum of six grid cells with valid values is used as a threshold for a valid standard deviation.

The melt flag is a near-real-time version of the Drobot and Anderson (2001) algorithm, which uses a brightness temperature difference threshold to determine whether melt has begun for the overlying snow cover at each sea ice grid cell. The algorithm is implemented as follows:

$$T_B(19H) - T_B(37H) > 2K \rightarrow \textit{no melt} \qquad (21)$$

$$T_B(19H) - T_B(37H) \leq 2K \rightarrow \textit{melt has begun} \qquad (22)$$

A long-term melt onset climate dataset, NSIDC-0105, is distributed by NSIDC (https://nsidc.org/data/nsidc-0105). That dataset includes a 20-day temporal filter to screen out possible false melt signatures. For simplicity, the temporal filter is not employed in this product. This means that some grid cells flagged as melt may not actually be melting, and thus, the flag is more conservative than the climate dataset. Note that the melt test does not consider any effects of sea ice motion.

The melt onset test is used starting on March 1 (DOY=60), around the time when the maximum sea ice extent is reached each year. Once a grid cell is flagged as melting, it remains so through the rest of the summer until September 1 (DOY=244), roughly the time when extent reaches its minimum value. When the sea ice concentration is zero, the flag will be turned off. In other words, the flag will only be on if melt conditions are met and there is sea ice. Note this is different from the melt_onset_day_seaice_conc_cdr variable which, once set, shows the day of melt onset through the rest of the year. Also note that melt may be intermittent initially in the spring (melt, then refreeze, and melt again) and freeze-up begins near the pole well before September 1. Thus, grid cells that are flagged as melt may not actually have melt occurring and the flag should be used only as a guide for the data quality of the CDR concentration estimates and should not be used specifically for studies on melt. Like the melt_onset_day_seaice_conc_cdr, the input F17 brightness temperatures are scaled. See the note in number 3, Day of Melt Onset, above for more details.

The melt algorithm is not run within two grid cells of the coast due to possible effects of mixed land-ice grid cells. The melt algorithm is also valid only for grid cells with concentrations of at least 50%. These are separately flagged as both situations (coast, low concentration) reflect regimes with likely higher errors.

Table 10 lists the flag values in the QA field, with an explanation for each parameter. Grid cells with more than one flag property contain the sum of both flags. In general, higher values are more likely to have high errors. Note that 0 is the fill value for this variable.

Condition	Flag Value	Label in NetCDF variable
BT source for CDR (BT > NT)	1	BT_source _for_CDR
NT source for CDR (NT > BT)	2	NT_source_for_CDR
Region masked by ocean climatology	4	no_ice_allowed_per_climatology
Grid cell near the coast	8	grid_cell_near_to_coast
Concentration < 50%	32	concentration_below_fifty_percent

Start of Melt Detected (Arctic only)	128	melt_start_detected

Table 10: List of flag values used in the daily CDR QA field. A grid cell that satisfies more than one criteria will contain the sum of all applicable flag values. For example, where the Bootstrap and NASA Team concentrations are equal and both are equally usable for the CDR concentration, the flag value will be 3 (1 for BT plus 2 for NT).

5. NASA Team Sea Ice Concentrations processed by Goddard (TCDR Only)

   For many years, NSIDC has distributed NASA Team sea ice concentrations processed at NASA Goddard (currently distributed at: https://nsidc.org/data/nsidc-0051). The Goddard NASA Team concentrations are generally updated once per year, approximately 3-6 months after the end of the year, though delivery of updates can vary.

   NSIDC includes this field, named goddard_nt_seaice_conc, in the finalized TCDR product suite to provide continuity for long-time NSIDC users who want to continue using NASA Team concentrations. In addition, the Goddard processing includes concentrations from the SMMR era, 1978-1987 and thus extends the length of the time series. NSIDC has not assessed provenance and processing methods for SMMR to include in the CDR field. NSIDC plans to add SMMR in a future version.

   Complete processing details of the NASA Team sea ice concentrations by Goddard are available in the documentation for Sea Ice Concentrations from Nimbus-7 SMMR and DMSP SSM/I-SSMIS Passive Microwave Data (https://nsidc.org/data/nsidc-0051).

6. Bootstrap Sea Ice Concentrations processed by Goddard (TCDR Only)

   NSIDC also has long distributed Bootstrap concentrations processed by Goddard (currently available at: https://nsidc.org/data/nsidc-0079). Similar to the NASA Team concentrations discussed above, we provide this field in the finalized TCDR product, named goddard_bt_seaice_conc, as a courtesy to long-time Bootstrap users. The brightness temperature source is the same as that used at NSIDC. There are also fewer differences between the Goddard and NSIDC Bootstrap processing. However, Bootstrap does include the spatial/temporal interpolation of missing values and the manual QC process. Note that Goddard has recently released Version 3 of their Bootstrap product. They have made minor adjustments to the Bootstrap algorithm that are described in Comiso et al. (2017). NSIDC has not made these adjustments to our processing of the bootstrap algorithm but will do so in a future release of this product.

Complete processing details of the NASA Team sea ice concentrations by Goddard are available in the documentation for Bootstrap Sea Ice Concentrations from Nimbus-7 SMMR and DMSP SSM/I-SSMIS (https://nsidc.org/data/nsidc-0079).

7. Combined Goddard Bootstrap/NASA Team Concentrations (TCDR Only)

   As an augmentation to the sea ice CDR, an analogous combined Goddard field, named goddard_merged_seaice_conc, is provided in the finalized TCDR product. This field uses the Goddard-processed Bootstrap and NASA Team concentrations as inputs and then uses the exact same methodology to create a combined field as is used for the sea ice CDR field. Thus, it includes the SMMR period (1978-1987) and hence a longer record. Also, it includes interpolation and manual QC that yield more complete and cleaner fields. This field uses a combined Southern Hemisphere land mask.

   While there are the noted processing differences between this combined field and the CDR field (Table 11), the differences are small enough such that the fields can be used interchangeably with reasonable confidence for large-scale studies (for example, long-term hemispheric sea ice extent trends). However, inconsistencies may occur when studying smaller regions. For the longest, most complete and most up-to-date time series, we recommend using the Goddard combined field (this field) augmented with the CDR field (No. 1 above) for the most recent data.

	CDR	**Goddard NT**	**Goddard BT**	**Goddard Merged**
NetCDF Parameter Name	seaice_conc_cdr	goddard_nt_ seaice_conc	Goddard_bt_ seaice_conc	Goddard_merged_seaice_ conc
Processing location	NSIDC	Goddard	Goddard	NSIDC, from Goddard products
Processing fully documented?	Yes	No	No	No
Accompanying data quality info?	Yes	No	No	No
Interpolation, Manual QC?	No	Yes	Yes	Yes

Beginning year of time series	1987	1978	1978	1978
Update frequency	NRT: Daily Final: approx. every 3 months	Approx. once per year	Approx. once per year	Approx. once per year
Usage	Consistent, fully-documented product	Historical NT users	Historical BT users	Extension of CDR back to 1978, enhanced QC

Table 11: Summary of differences between provided concentration fields and guidance for use.

3.4.4.2 Fields in the monthly CDR files

The monthly fields are created from all daily files in the given month. The TCDR and ICDR both contain sea ice concentration, standard deviation, melt onset, and quality assessment fields, but the TCDR contains an extra three ancillary fields.

1. seaice_conc_monthly_cdr
2. stdev_of_seaice_conc_monthly_cdr
3. melt_onset_day_seaice_conc_monthly_cdr
4. qa_of_seaice_conc_monthly_cdr
5. goddard_nt_seaice_conc_monthly (TCDR only)
6. goddard_bt_seaice_conc_monthly (TCDR only)
7. goddard_merged_seaice_conc_monthly (TCDR only)

These CDR fields are explained below:

1. Sea Ice Concentration CDR

   This field, named seaice_conc_monthly_cdr, contains the monthly average sea ice concentration values for the CDR, scaled from 0-100%. This field (and the standard deviation and QA fields discussed below) is processed entirely at NSIDC with all processing steps fully documented. For the TCDR, it includes the entire SSM/I-SSMIS time series, 1987-present. For the ICDR, it includes SSMIS for the NRT data. The flag values for the sea ice concentration variables are the same as for the daily fields given in Table 10.

   The monthly average is computed at each grid cell by averaging all available daily values in the month for that grid cell. A minimum of 20 days is required for a valid monthly value. If a grid cell has fewer than 20 days with non-missing data, that grid cell is assigned the missing flag in the monthly field. No concentration threshold is used in the monthly fields – i.e., unlike the daily fields, monthly concentration values of less than 10% may occur.

2. Standard Deviation of Concentration

   This field, named stdev_of_seaice_conc_monthly_cdr, contains the standard deviation (with one degree of freedom) of the daily concentrations in the month. As in the monthly concentration, a minimum of 20 days is required for a valid monthly value. Note that while the daily concentration standard deviation field is based on the variability of the NT and BT concentrations over a 3 x 3 grid cell spatial region, this monthly field is simply the standard deviation of the daily CDR concentrations – i.e., a temporal standard deviation for each grid cell.

3. Day of Melt Onset

   This field, named melt_onset_day_seaice_conc_cdr, contains the day of year on which melting sea ice was first detected in each grid cell. Once detected, the value is retained for the rest of the year. For example, if a grid cell started melting on day 73, the variable for the grid cell on that day will be 73, as will all subsequent days until the end of the year. The melt onset day is only calculated for the melt season: days 60 through 244, inclusive. Before melting is detected or if no melt is ever detected for that grid cell, the value will be -1 (missing / fill value).

   The conditions for melt onset at a particular grid cell are the following:

   - Melt detected:
     - Concentration >= 50% at the beginning of the season
     - Grid cell is not land, coast, shore (1 grid cell from coast), near-shore (2 grid cells from coast), or lake
   - Current sea ice concentration >= 50%
   - Brightness temperature delta (19H - 37H) < 2K
   - Presence of brightness temperatures for both channels (19H, 37H)

   Note: To calculate the melt onset for F17 data (2008 – present), the input brightness temperatures are first scaled as follows:

   $$19H\_scaled = 1.021 * 19H - 1.681 \qquad \textit{(19, previously listed)}$$

   $$37H\_scaled = 1.001 * 37H - 0.650 \qquad \textit{(20, previously listed)}$$

   These equations were derived by a regression between F17 and F13 brightness temperatures during March through September 2007 when there was an overlap period between the two satellites. Regressions were run for each daily average brightness temperature field and slope and intercept values were calculated.

These daily slope and intercept values were then averaged over the entire March through September period to derive the equations above.

The reason for applying this adjustment is to account for differences between the F17 and F13 sensors, including sensor characteristics (sensor footprint, geometry), differences in orbit (time of equatorial crossing), etc. For the NASA Team sea ice concentration algorithm, the differences between the two sensors are accounted for by adjusting the algorithm tie-points (Cavalieri et al., 2011). For the Bootstrap sea ice concentration algorithm, only a regression is needed because tie-points are derived daily from the brightness temperature fields. For the melt onset, Equations 19 and 20 are used to make this adjustment.

4. Quality Assessment Flags

This field, named qa_of_seaice_conc_monthly_cdr, contains flags indicating the potential quality of monthly averages. The flags are listed in Table 12 and generally follow the same approach as the daily flags, noting the primary source (NT or BT) of the CDR, areas masked by ocean climatology (i.e., no sea ice allowed), grid cells near the coast, ice occurrence, and melt state. There are some differences with the daily QA field however. First, for NT and BT as a source, for the monthly field the flag is assigned for each grid cell for which field was used for the majority of the month – i.e., which algorithm was most used for the monthly average. Also, instead of flag concentrations less than 50%, a flag is assigned to cells that had ice (concentration > 0%) less than half of the month. This helps a user assess whether the monthly average is indicative of a temporal change in the presence of ice cover. For melt, two flags are included: one for the detection of melt in any day during the month, and the other for the presence of melt in a grid cell for more than half of the month. Since melt tends to bias concentrations lower, these two flag values give a sense of whether melt has any effect on the monthly concentration estimate and whether it is having a dominating effect.

Note: Like the melt_onset_day_seaice_conc_monthly_cdr, the input F17 and F18 brightness temperatures for the melt_detected_at_least_one_day and melt_detected_greater_than_half_month flags are scaled. See the note in number 3, Day of Melt Onset, above for complete details.

Condition	**Flag Value**	**Label in NetCDF File**
Number of BT > Number of NT	1	BT_majority_algorithm_for_monthly_CDR
Number of NT > Number of BT	2	NT_majority_algorithm_for_monthly_CDR

Region masked by ocean climatology	4	no_ice_allowed_per_climatology
Grid cell near the coast	8	grid_cell_near_to_coast
Ice present < 50%	32	ice_present_less_half_of_month
melt detected >= 1	64	melt_detected_at_least_one_day
Melt detected > 50%	128	melt_detected_greater_than_half_month

Table 12: List of flag values used in the daily CDR QA field. A grid cell that satisfies more than one criteria will contain the sum of all applicable flag values. For example, where the Bootstrap and NASA Team concentrations are equal and both are equally usable for the CDR concentration, the flag value will be 3 (1 for BT plus 2 for NT).

5. NASA Team Monthly Concentrations Processed by Goddard (TCDR Only)

   The original monthly NASA Team concentrations, processed by Goddard, and created by Goddard from their daily concentrations are provided in the field named goddard_nt_seaice_conc_monthly in the finalized TCDR product. The monthly CDR concentration processing and averaging follows the same procedure as done at Goddard.

6. Bootstrap Monthly Concentrations Processed by Goddard (TCDR Only)

   The original monthly Bootstrap concentrations, processed by Goddard, and created by Goddard from their daily concentrations are provided in the field named goddard_bt_seaice_conc_monthly in the finalized TCDR product. The monthly CDR concentration processing and averaging follows the same procedure as done at Goddard. Note that Goddard has recently released Version 3 of their Bootstrap product. They have made minor adjustments to the Bootstrap algorithm that are described in Comiso et al. (2017). NSIDC has not made these adjustments to our processing of the bootstrap algorithm but will do so in a future release of this product.

7. Combined Goddard Bootstrap/NASA Team Concentrations (TCDR Only)

   As for the daily fields, an augmentation to the monthly sea ice CDR is done by combing the Bootstrap and NASA Team fields into an analogous combined Goddard field, named goddard_merged_seaice_conc_monthly in the finalized TCDR product. This combines the Goddard-processed NASA Team and Bootstrap monthly fields in the same way as the daily CDR fields are produced. Small differences between Goddard merged and the CDR are present because Goddard interpolates missing data in daily fields (so the number of daily fields in

a grid cell will always be a full month and a 20 day threshold is not required. Other minor processing difference may yield small differences in concentrations. However, the differences are smaller than in the daily fields and small enough so that these combined fields can be used interchangeably with the CDR monthly fields to extend the temporal coverage back to the beginning of the SMMR period in 1978.

4. Test Datasets and Outputs

4.1 Test Input Datasets

The TCDR is both tested against and includes within, two existing, widely available data sets. These are *NSIDC-0051: Sea Ice Concentrations from Nimbus-7 SMMR and DMSP SSM/I Passive Microwave Data* (https://nsidc.org/data/nsidc-0051) and *NSIDC-0079: Bootstrap Sea Ice Concentrations from Nimbus-7 SMMR and DMSP SSM/I* (https://nsidc.org/data/nsidc-0079).

We worked directly with GSFC and have incorporated some of their code and data into the CDR production. Within the confines of producing a CDR, we have recreated, as accurately as possible, the existing data sets as published before implementing the CDR algorithm.

The near-real-time ICDR product follows the same methodology as the standard TCDR, only run with near-real-time input brightness temperatures. Comparisons between NRT and final sea ice concentration algorithms indicates good agreement between the two, with daily extent and area differences generally below 50,000 square kilometers and overall average differences of 20,000 – 30,000 square kilometers. These are generally <1% of the overall extent and average. Nonetheless, the NRT data should be considered provisional, and it is recommended that only final data be used for climate monitoring.

4.2 Test Output Analysis

4.2.1 Reproducibility

The test results can be verified by running the algorithm with the same input T_Bs and the same ancillary fields and then checking to ensure the results are the same. This has been done in Peng et al. (2013) and Meier et al. (2014) to verify that the CDR algorithm can reasonably reproduce the original concentration fields provided by NASA Goddard. They show that CDR algorithms are able to reproduce the original Goddard algorithms, except for small difference due to known processing variations (for example, filling missing data, manual quality control).

4.2.2 Precision and Accuracy

The precision and accuracy of the algorithms have been evaluated in numerous studies over the years (for example, Cavalieri et al., 1991; Comiso et al., 1997; Kwok, 2002; Meier, 2005; Andersen et al., 2006, 2007; Ivanova et al., 2014). Overall, the algorithm has a precision of ~5% with an accuracy of ~10%. However, uncertainties are higher under some conditions – most notably near the ice edge and when the surface is undergoing melt. In addition, while filters remove many artifacts (see above), some erroneous ice can still occur over the open ocean due to weather effects and along the coast due to land spillover effects (i.e., mixed ocean and land grid cells).

4.2.3 Error Budget

Much of the error is attributable to the limitations of the source data. First, the spatial resolution of the input sensor data is limiting. Some input brightness temperature sensor footprints have an effective resolution of ~70 km x ~45 km. This means that any variability below this resolution (for example, the location of the ice edge) may be missed. The sensor resolution is also the cause of the land spillover issue, where a sensor footprint incorporates a mixture of land and open water, which in some conditions has a signature that is interpreted by the algorithm as sea ice.

There are more modern sensors, such as the Advanced Microwave Scanning Radiometer (AMSR). However, these records only go back to 2002, so they are not suitable for a long-term CDR. A recently-developed, gridded brightness-temperature product includes a resolution enhancement technique using multiple satellite overpasses to improve gridded resolution from 25 km to 6.25 km. This may reduce the land-spillover effect and improve ice edge detection.

Another limitation is surface melt. Passive microwave sensors are sensitive to the phase state of water (liquid or solid), which allows the algorithms to distinguish between sea ice and ocean. However, because the microwave emission comes from at or near the surface, water on the surface of the ice is interpreted as liquid. This causes the algorithms to underestimate concentration when ice is melting. The algorithms can be potentially adjusted to reduce this, but then they tend to overestimate concentration during non-melt conditions. Dynamic (automatically varying) daily tie-points can alleviate this effect some by allowing the algorithm to adjust to different surface conditions.

Error	**Magnitude**	**Description**
Inter-satellite bias	<0.5% of total sea ice extent and area	Inter-calibration has been done to minimize differences in algorithm outputs. Analysis of inter-calibrated retrievals show small differences (Cavalieri et al., 1999; 2012).

		However, some overlap periods were short and during periods (summer) of high variability. Thus, quantitative values may underestimate the true bias.
Diurnal correction	Undetermined/minimal	Daily average T_B fields are used, which removes most diurnal effects. Different sensors have different orbits that result in some diurnal impacts, but these are implicitly addressed in the satellite intercalibration, which reduces such effects to near zero over most of the ice pack, though larger effects can occur in narrow band near the ice edge.
Unknown calibration drifts	Undetermined/minimal	This has not been investigated in detail. No evidence of significance has been observed and comparison with other sensors (AMSR-E) indicate that drift effects are negligible.
Effect of changes in surface properties	Undetermined	The sea ice algorithms are sensitive to surface conditions and tend to underestimate concentration during melt and for new ice. As melt is occurring earlier and is more widespread, errors in concentration and area trends may result. This has not been investigated in detail.

Table 13: Possible error sources and magnitudes for the sea ice CDR

5. Practical Considerations

5.1 Numerical Computation Considerations

No parallelization or difficulties in matrix inversions are expected. Round-off errors exist in conversions between data types (floating point to byte and the reverse), but these are expected and well within the tolerance of the current algorithm and instrument accuracy.

5.2 Programming and Procedural Considerations

Daily processing is independent and can be run in parallel, except for the melt algorithm information, which must be run as a post processing step.

Numerical Python (NumPy) is required for CDR processing. Python module, unittest2, is used in testing.

5.3 Quality Assessment and Diagnostics

Researchers can assess and improve a CDR by comparing it with operational products. Absolute error can be approximated via comparison to operational sea ice products, such as those produced by the U.S. National Ice Center or the Canadian Ice Service; but it is important to keep in mind that such products have an operational focus different from the climate focus of the CDR, and the two are not expected to be consistent with each other. The documentation for the daily Multi-sensor Analyzed Sea Ice Extent (MASIE) (https://nsidc.org/data/masie), distributed by NSIDC in cooperation with NIC, gives a summary of how satellite passive microwave CDRs differ from operational products.

5.4 Exception Handling

If a subprocess failure occurs, the code raises an **OsError** which is caught; and the program exits with an error.

Failure to create a working directory will raise an **OSError** and exits the program.

Any missing data files raise an **IOError** and exits the program.

5.5 Algorithm Validation and Error Assessment

Several studies over the years have assessed ice concentration estimates from the NASA Team and Bootstrap algorithms. These assessments have typically used coincident airborne or satellite remote sensing data from optical, thermal, or radar sensors, generally at a higher spatial resolution than the SSM/I and SSMIS instruments but with only local or regional coverage. Several assessments indicate an accuracy of approximately 5% during mid-winter conditions away from the coast and the ice edge

(Steffen et al., 1992; Gloersen et al., 1993; Comiso et al., 1997; Meier et al., 2005; Andersen et al., 2007, Belchansky and Douglas, 2002). Other assessments suggest concentration estimates are less accurate. Kwok (2002) found that passive microwave overestimates open water by three to five times in winter. Partington et al. (2003) found a difference with operational charts that was relatively low in the winter but rose to more than 20% in summer. Errors can come from problems with the sensor, from weather effects, and from inadequacies in the algorithm. For example, a satellite's orbit may drift over time, which may degrade an instrument's data quality. Most SSM/I instruments were in use long past their designed lifetime expectancy. Atmospheric water vapor is a weather effect that can modulate the passive microwave signature of the surface, particularly at the 19 GHz frequency, causing ice concentration to be overestimated. Finally, while the emissivity of seawater is quite constant, that of sea ice varies considerably depending on many factors including age, thickness, and surface roughness. When one considers that algorithms must arrive at a single number for ice concentration taking into account the varying brightness temperatures of all the different surface types that may fill the footprints of the 19 GHz and 37 GHz channels and that those footprints differ in size and shape across the instrument swath, one can appreciate the difficulty of the problem. *Microwave Remote Sensing of Sea Ice*, F. Carsey, editor, is a comprehensive overview of the subject (Carsey, 1992).When melt ponds form on the surface of ice floes in the summer, the ice concentration appears to decline when in fact the true concentration may not have changed (Fetterer and Untersteiner, 1998). Melt state is a surface effect that may in itself contain a climate trend, which could influence sea ice concentration trend estimates. This and other concentration error sources have been examined to some extent in Andersen et al. (2007), and their influence appears to be small compared to the estimated sea ice trends, but such effects should be kept in mind when using these data.

5.5.1 Errors from sensor characteristics and gridding scheme

There are four errors that come from the sensor characteristics: (A) sensor noise, (B) the transition between sensors, (C) the large IFOV of the sensors, and (D) the 24-hour composite.

A. One source of error is simply from sensor noise. The SSM/I and SSMIS sensors have been found to have an RMS error of 0.5 K to 1.0 K (Wentz, 1997). A sensitivity study of NASA Team algorithm concentration (https://nsidc.org/data/pm/nasateam-index) found that the concentration sensitivity is about 1-2% per 1 K (Gloersen et al., 1993). Thus, the algorithm precision is about 1%.

B. Another potential sensor error results from the transition between sensors on different platforms. The brightness temperature regression and tie-point adjustment corrects for this, though small artifacts remain (Cavalieri et al., 1999; Comiso and Nishio, 2008). Comparison of ice extent estimates from sensor overlap periods indicate that the adjustments yield agreements that are on the order of 0.05% or less and about 0.5% for sea ice area (Cavalieri et al., 1999;

Cavalieri et al., 2011). Short overlap periods of early sensor transitions (SMMR to F8 and F8 to F11) may not account for the full seasonal variability (Meier et al., 2011; Cavalieri et al., 2011) and differences may be higher in some cases. However, differences appear to be well below the sensitivity of the instrument, thus, providing confidence in the robustness of the intercalibrated algorithms through the time series.

C. A more significant limitation of the sensors are the large sensor footprint (IFOV) of the SSM/I and SSMIS channels. Though all input brightness temperatures are gridded to the 25 km polar stereographic grid, the IFOV of the sensor is coarser than this (Table 2), as low as 70 x 45 km for the 19.35 GHz channel. This means that the sensor is obtaining information from up to a 3 x 2 grid cell (75 km x 50 km) region, but because a simple drop-in-the-bucket gridding method is used, that signature is placed in a single grid cell. This results in a spatial “smearing” across several grid cells. Also, some grid cells do not coincide with the center of the sensor footprint and are, thus, left as missing even though there is brightness temperature information available at that region. This effect also causes the land-spillover issue of grid cells with a mixture of land and water brightness temperatures that can be interpreted by the algorithms as sea ice.

D. Another issue is the use of 24-hour composite average brightness temperatures as input for the concentration algorithms. Sea ice can drift with the winds and ocean currents over a 24-hour period, and the surface properties of the sea ice can also change considerably. Thus, the daily brightness temperature fields of the surface properties at a given grid cell are an amalgamation of conditions over 24 hours.

   Some of the effect caused by this spatial and temporal compositing of the brightness temperatures is ameliorated because these data have been used consistently for algorithm development, tie-point derivation, intersensor adjustment, and all processing. Thus, these effects, while limiting accuracy on a grid cell level, still yield consistent large-scale trends and variability in the sea ice cover. Regions with sharp gradients in brightness temperature, such as the ice edge and the land/water boundary, are most affected by these characteristics.

   Of particular note is the compositing effect on the precision of the ice edge. First, the ice edge is a region of sharp brightness temperature gradients and rapid (less than 24 hour) variability. Second, there is necessarily ambiguity in the ice edge location due to the limited spatial resolution. For example, an ice edge grid cell (that is, the adjoining grid cells are ice-free) with a 50% concentration could mean that the entire cell has a uniformly distributed 50% ice concentration, that half of the grid is covered by 100% ice and the other half is ice free, or something in between. Because the true spatial resolution is limited by the sensor IFOV and not the grid cell area, even with perfect data and a perfect algorithm, the ice edge can in principle only be discerned to within ~50 km. However, the distance between the passive microwave observed (15%

concentration) edge and the true ice edge, as determined in ship observations (Ozsoy-Cicek et al., 2009; Ozsoy-Cicek et al., 2011), operational sea ice charts (Partington, 2000), or high resolution satellite data (Meier et al., 2003; Meier, 2005), may be much larger than that.

5.5.2 Errors due to surface variation and ambiguities

There are four primary error sources from surface variation and ambiguities: (A) ice type, (B) ice surface variation, (C) physical temperature, and (D) surface melt.

A. While five passive microwave channels are potentially available for discriminating sea ice, not all are completely independent and in practice only three surface types are retrievable, one water and two ice (multi-year and first-year). However, two ice types cannot fully describe the complex surface of the sea ice. Tie-points are derived based on “pure surface types” of 100% ice, typically for thick multi-year or first-year ice (for the Arctic). The actual emission from thin ice (as indicated by the brightness temperature) varies with ice thickness up to perhaps 30 cm. Thus, thin ice cover appears in the algorithms as a mixture of water and thick ice. So, thin ice concentration is often underestimated. Algorithms using specific thin ice tie-points have been developed (Cavalieri et al., 1994), but these are not applicable for hemispheric datasets. Because ice quickly grows thicker in winter months, thin ice tends to constitute a small fraction of the overall ice cover, but can result in large error near the ice edge and regions dominated by thin ice (such as the Sea of Okhotsk). Validation studies indicate that the Bootstrap algorithm is more sensitive to thin ice, and thus, more accurate in those regions than the NASA Team algorithm (Partington, 2000).

B. Beyond thin ice, other sea ice surface variability factors impact the brightness temperature signal, including snow cover, frost flowers, and variations in ice salinity. During winter conditions, these effects are generally small, resulting in average concentration errors of a few percent (Gloersen et al., 1993), though higher errors can occur and are most often underestimations. For example, a comparison between passive microwave sea ice concentrations and concentration derived from high-resolution SAR scenes found that SAR showed less than 0.5% open water area in winter mid-pack sea ice while Bootstrap and NASA Team estimates had 1-3% open water.

   Algorithms have been developed to also employ the higher frequency channels (85.5 GHz on SSM/I) to provide additional information (Markus and Cavalieri, 2000; Spreen et al., 2008). However, these algorithms typically require ancillary atmospheric data and/or radiative transfer modeling because the high frequency channels are more sensitive to atmospheric emission. Also, the high frequency data have anomalies in the early part of the time series, limiting the length of the record, and unlike the lower frequency channels, are not available at all for the 1978-1987 SMMR record.

C. Physical temperature can also cause errors in the sea ice retrieval. Brightness temperature is a function of both the surface emissivity and the physical temperature. So, changes in physical temperature change the retrieved brightness temperature and hence the concentration. The algorithm tie-points implicitly account for a physical temperature, but large variations in temperature can cause errors. The Bootstrap algorithm concentrations have a low bias in extremely cold conditions, typically during the mid-winter season in the high Arctic and near the Antarctic coast. Use of daily tie-points limits this effect, but estimates are still biased low. The NASA Team algorithm uses brightness temperature ratios, so the effect of physical temperature largely cancels out within the algorithm equations.

D. The largest surface effect on the retrieved concentration accuracy is surface melt. When the snow cover overlying the sea ice begins to melt, the microwave emission changes significantly because of the different emissive properties of water in the frozen state versus the liquid state (Eppler et al., 1992). The brightness temperature values over melting snow and ice are effectively interpreted by the algorithms as a mixture of sea ice and open water. The effect is further exacerbated when melt ponds form on the surface of the ice. Thus, a substantial low bias in summer concentrations of 20-30% from both NASA Team and Bootstrap algorithms has been found in numerous studies (Agnew and Howell, 2003; Gloersen et al., 1993; Cavalieri, 1994; Comiso et al., 1997; Partington, 2000; Meier, 2005)

5.5.3 Errors due to atmospheric effects

A significant advantage of passive microwave data for sea ice concentration retrieval is that atmospheric emission is typically in the SSM/I and SSMIS frequencies used in the algorithms. This provides all-sky capabilities and allows satellite passive microwave sensors to obtain complete, daily sea ice concentration fields.

However, while atmospheric emission or atmosphere-induced surface emission is typically small, it can cause significant errors in some situations. The atmosphere primarily affects the algorithms over open water and thin ice.

The first effect is not direct emission by the atmosphere but an induced effect. Wind blowing over the ocean roughens the surface, which increases the emission. Even a relatively light wind (for example, 5 m/s) can increase emission enough to register several percent concentration of sea ice when no ice is present (Gloersen et al., 1993; Andersen et al., 2006). The use of weather filters and a 15% concentration threshold eliminates most, but not all, wind effects.

The primary atmospheric emission sources are water vapor and liquid water in clouds. These sources also increase the emission retrieved by the sensor and serve to erroneously increase ice concentration. Sensitivity studies indicate that these effects can be up to a 10-20% concentration bias for open water, with decreasing effects as

sea ice concentration increases (Maslanik, 1992; Oelke, 1997; Andersen et al., 2006). Thus, such effects are primarily limited to open water and near-edge sea ice grid cells. The weather filters and the 15% threshold remove much of the effect over water, but some artifacts may remain.

5.5.4 Summary of error sources and magnitudes

Table 14 summarizes the error sources, expected potential magnitude of the error, the spatial and/or temporal regime, and the relative effect on each algorithm (BT, NT). These are ranges of typical values as reported in the cited validation studies. Errors at any given grid cell may be larger. Note that many errors will be mitigated in the monthly average fields. Thus, monthly averages are generally more accurate and more stable and are better suited for climate analyses.

Error Source	Typical Magnitude and bias (if any)	Spatial/Temporal Regime	Relative Effect on Algorithm
Sensor Noise	+/-1%	All	NT and BT
IFOV/Gridding	<5%	Winter, pack ice	NT and BT
IFOV/ Gridding	0-100%	Sharp gradients (e.g., ice edge, coast)	NT and BT
Intersensor calibration	~0.1%	All	NT and BT
Physical temperature	<5%, low	Winter, cold	BT more than NT
Non-melt surface variation	<5%, low	Winter, central pack ice	NT more than BT
Thin ice	~30-50%, low	Near ice edge, fall freeze-up	NT more than BT
Surface melt	~10-30%, low	Summer	NT more than BT
Wind	5-20%, high	Open water	NT and BT
Water Vapor, Liquid Water	0-20%, high	Open water and ice near edge	NT and BT

Table 14: List of error sources and typical magnitudes for the NASA Team (NT) and Bootstrap (BT) algorithms with biases and typical regimes.

5.6 Processing Environment and Resources

The CDR code is run on a 2.4 GHz 64-bit Xeon VSphere virtual machine, running Ubuntu 14.04 LTS (GNU/Linux 3.13.0-24-generic x86_64), with 3 GB of RAM, fiber mounted, and NFS mounted disks. A day's worth of data can be processed on a single CPU in about one minute (wall time).

The complete install memory requirements are approximately 350 MB. This includes the code package, the input and output data, and all ancillary files such as masks and configuration files. The daily processing produces approximately 12 MB ICDR or 14 MB TCDR of temporary files that are deleted by mechanisms in the code when processing is complete.

File Type	Size
Code package	85 MB
TCDR Input files	Northern hemisphere: 1.7 MB/day Southern hemisphere: 1.3 MB/day
TCDR Daily output files	Northern hemisphere: 2.5 - 3.7 MB/file/day Southern hemisphere: 1.8 - 2.5 MB/file/day
TCDR Monthly output files	Northern hemisphere: 3.7 MB/file/month Southern hemisphere: 2.9 MB/file/month
ICDR Input files	Northern hemisphere: 2.7 MB/day Southern hemisphere: 2.1 MB/day
ICDR Daily output files	Northern hemisphere: 3.0 - 3.4 MB/file/day Southern hemisphere: 1.8 - 2.4 MB/file/day
ICDR Monthly output files	Northern hemisphere: 3.4 MB/file/month Southern hemisphere: 2.6 MB/file/month
Ancillary files	93 MB

Table 15: Install memory requirements

The following libraries are required to run the cdr_daily_seaice.py and cdr_monthly_seaice.py routines.

Core/Python Libraries:

The code is packaged as a conda package. As such, the required Linux and Python packages are installed at the same time. All of the libraries listed below are installed from the conda-forge (https://conda-forge.github.io/feedstocks), the mutirri channel (https://anaconda.org/mutirri/repo?type=conda&label=main), or the NSIDC channel (https://anaconda.org/nsidc/repo?type=conda&label=main).

- invoke
- netcdf4=1.1.9
- nose
- nose-exclude
- rednose

- mock
- flake8
- ply
- cdlparser
- pyfdistill
- szip=2.1
- numpy
- nsidc0622-valid-ice-mask-to-binary=1.1.0
- jupyter
- matplotlib

6. Assumptions and Limitations

As noted elsewhere, a primary limitation is the spatial resolution (sensor footprint) of the input data, which limits the detail that can be retrieved by the algorithm. The product is on a 25 km (nominal) resolution grid, but some input data has a resolution as ~70 km x ~45 km. This means that small-scale features are not explicitly resolved by the algorithm and the precision of the ice edge location is limited to ~25 km at best. This is generally not sufficient for operational support (for example, navigational guidance) and the product should not be used for such purposes. The primary application of the product is for long-term climate monitoring and general guidance on overall regional and global sea ice concentrations, not operational and/or local applications.

6.1 Algorithm Performance

The algorithm is empirically derived based on the microwave emission of pure surface types. Because of the number of sensor frequency and polarization combinations that are completely independent, only three surface types can be discriminated by the algorithm – two for sea ice and one for open water. However, the sea ice surface in particular, is highly heterogeneous. The microwave signature of ice varies based on ice thickness (up to ~50 cm), snow cover, and melt state. For a global, long-term algorithm, the algorithm is tuned to thick, cold sea ice conditions. This means that the algorithm tends to underperform in regions of thin ice and during melt conditions. Heavy snow cover can also impact the algorithm retrieval, especially if the snow grain size changes significantly and/or there are melt/re-freeze events. Over open water, ocean waves and/or atmospheric emission (especially by liquid water clouds) can increase the surface emission signal and result in false ice retrieval. Weather filters (discussed above in the NASA Team Weather Filters and Bootstrap Weather Filters sections) have been included to ameliorate as much of these effects as possible, but occasionally some false ice can still occur.

6.2 Sensor Performance

The sensor performance is dependent on operations by the DMSP. Radiometic calibration between sensor transitions is corrected by the sensor-specific tie-point adjustments used by the algorithm, but changes in calibration within a sensor are not addressed. The concentration fields are monitored and sudden changes are an indication of changes in calibration or other sensor malfunction. Generally, these spurious changes have been short-lived, but when they are chronic, the algorithm can be transitioned to use a new sensor. Radiometric noise for the passive microwave sensors has not been an issue.

7. Future Enhancements

Other enhancements in the sea ice concentration CDR will be considered for the future, pending available funding. Some of the main potential enhancements are discussed below.

7.1.1 Reprocessing of SSM/I using RSS Version 7 brightness temperatures

The current CDR product is based on multiple versions of RSS brightness temperatures. See Table 3. The intersensor adjustments between F13 and F17 were made using these versions of brightness temperatures, so any differences in RSS versions should be accounted for within the algorithm intersensor adjustments. However, we aim to do a full reprocessing with Version 7 for all SSM/I and SSMIS data at NSIDC and will reprocess the sea ice product when resources allow.

7.1.2 Reprocessing of SMMR brightness temperatures and extension of CDR field to 1978

The current CDR does not include the SMMR product because full provenance and documentation of the SMMR brightness temperatures and the processing methodology (for example, manual filtering of bad grid cells) cannot be assured. According to NASA Goddard (C. Parkinson, personal communication), there were many issues with the original SMMR data and many corrections were required). The SMMR time series is available as part of the Goddard NASA Team, Bootstrap, and (for extension of the sea ice TCDR) a combined field from the Goddard inputs. When resources allow, the SMMR sea ice record will be reprocessed, using an improved SMMR brightness temperature source.

7.1.3 EASE-Grid version of sea ice CDR

The CDR product will be integrated with other climate records, including the NOAA snow CDR and NASA MEaSUREs snow and sea ice Earth Science Data Records, both currently under development. As part of this effort, an EASE-Grid version will be produced, either via a re-gridding of the polar stereographic product or by processing the CDR algorithms on EASE-Grid brightness temperatures. Which method is used will depend on the availability of EASE-Grid brightness temperatures and resources.

8. References

Agnew, T., and S. Howell (2003). The use of operational ice charts for evaluating passive microwave ice concentration data. *Atmos. Ocean*, 41(4): 317-331.

Andersen, S., R. Tonboe, S. Kern, and H. Schyberg (2006). Improved retrieval of sea ice total concentration from spaceborne passive microwave observations using numerical weather prediction model fields: An intercomparison of nine algorithms. *Rem. Sens. Env.*, 104: 374-392.

Andersen, S., R. Tonboe, L. Kaleschke, G. Heygster, and L.T. Pedersen (2007). Intercomparison of passive microwave sea ice concentration retrievals over the high-concentration Arctic sea ice. J. Geophys. Res., 112, C08004, doi:10.1029/2006JC003543.

Belchansky, G.I., and D.C. Douglas (2002). Seasonal comparisons of sea ice concentration estimates derived from SSM/I, OKEAN, and RADARSAT data. Rem. Sens. Environ., 81: 67-81.

Cavalieri, D.J., P. Gloersen, and W.J. Campbell (1984). Determination of sea ice parameters with the NIMBUS-7 SMMR. *J. Geophys. Res*., 89(D4): 5355-5369.

Cavalieri, D. J., J. P. Crawford, M. R. Drinkwater, D. T. Eppler, L. D. Farmer, R. R. Jentz, and C. C. Wackerman (1991). Aircraft Active and Passive Microwave Validation of Sea Ice Concentration From the Defense Meteorological Satellite Program Special Sensor Microwave Imager. *J. Geophys. Res.*, 96(C12): 21989–22008.

Cavalieri, D. (1994). A microwave technique for mapping thin sea-ice. *J. Geophys. Res.*, 99(C6), 12561-12572.

Cavalieri, D., C. Parkinson, P. Gloersen, J. Comiso, and H. J. Zwally (1999). Deriving Long-term Time Series of Sea Ice Cover from Satellite Passive-microwave Multisensor Data Sets. *J. of Geophys. Res.,* 104(C7):15,803-15,814.

Cavalieri, D., C. Parkinson, N. DiGirolamo, A. Ivanov (2011). Intersensor calibration between F13 SSM/I and F17 SSMIS for global sea ice data records. *IEEE Geosci. Remote Sens. Lett*., 9(2), 233-236, doi:10.1109/LGRS.2011.2166754.

Cho, K., N. Sasaki, H. Shimoda, T. Sakata, and F. Nishio (1996). Evaluation and Improvement of SSM/I Sea Ice Concentration Algorithms for the Sea of Okhotsk. *J. Rem. Sens. of Japan,* 16(2):47-58.

Comiso, J.C. (1986). Characteristics of arctic winter sea ice from satellite multispectral microwave observations. *J. Geophys. Res*., 91(C1): 975-994.

Comiso, J. C., D. Cavalieri, C. Parkinson, and P. Gloersen (1997). Passive Microwave Algorithms for Sea Ice Concentrations: A Comparison of Two Techniques. *Rem. Sens. of the Environ.,* 60(3):357-384.

Comiso, J. C., and F. Nishio (2008). Trends in the Sea Ice Cover Using Enhanced and Compatible AMSR-E, SSM/I, and SMMR Data. *J. of Geophys. Res.,* 113, C02S07, doi:10.1029/2007JC0043257.

Comiso, J. C. (2009). Enhanced Sea Ice Concentrations and Ice Extents from AMSR-E Data. *J. Rem. Sens. of Japan,* 29(1):199-215.

Comiso, J.C., R.A. Gersten, L.V. Stock, J. Turner, G.J. Perez, and K. Cho. 2017. Positive Trend in the Antarctic Sea Ice Cover and Associated Changes in Surface Temperature. J. Climate, 30, 2251–2267, https://doi.org/10.1175/JCLI-D-16-0408.1

Drobot, S. and M. Anderson (2001). Comparison of Interannual Snowmelt Onset Dates with Atmospheric Conditions. *Annals of Glaciology* 33: 79-84.

Eppler, D.T., and 14 others (1992). Passive microwave signatures of sea ice, in "Microwave Remote Sensing of Sea Ice." F.D. Carsey, ed., *American Geophysical Union Monograph* 68, Washington, DC:47-71.

Gloersen, P., W.J. Campbell, D.J. Cavalieri, J.C. Comiso, C.L. Parkinson, and H.J. Zwally (1993). Arctic and Antarctic sea ice, 1978-1987: Satellite passive-microwave observations and analysis. *NASA Spec. Publ.* 511, 290 pp.

Hallikainen, M., and D.P. Winebrenner (1992). The physical basis for sea ice remote sensing, in "Microwave Remote Sensing of Sea Ice", F.D. Carsey, ed., *American Geophysical Union Monograph* 68, Washington, DC:29-46.

Hollinger, J., R. Lo, G. Poe, R. Savage, and J. Pierce (1987). Special Sensor Microwave/Imager User's Guide. *Naval Research Laboratory Report*, Washington, DC.

Ivanova, N., O.M. Johannessen, L.T. Pedersen, and R.T. Tonboe (2014). Retrieval of Arctic sea ice parameters by satellite passive microwave sensors: A comparison of eleven sea ice concentration algorithms, IEEE Trans. Geosci. Remote Sens., 52(11), 7233-7246, doi:10.1109/TGRS.2014.2310136.

Kunkee,D.B., G.A. Poe, D.J. Boucher, S.D. Swadley, Y. Hong, J.E. Wessel, and E.A. Uliana (2008). Design and evaluation of the first Special Sensor Microwave Imager/Sounder. *IEEE Trans. Geosci. Remote Sens*., 46(4), 863-883.

Kwok, R. (2002). Sea ice concentration estimates from satellite passive microwave radiometry and openings from SAR ice motion. *Geophys. Res. Lett*., 29(9), 1311, doi:10.1029/2002GL014787.

Levitus, S. and Boyer, T.P (1994). World Ocean Atlas 1994, Volume 4: Temperature, NOAA National Oceanographic Data Center, Ocean Climate Laboratory, U.S. Department of Commerce, Washington D.C.

Markus, T., and D.J. Cavalieri (2000). An enhancement of the NASA Team sea ice algorithm. *IEEE Trans. Geosci. Remote Sens*., 38(3): 1387-1398.

Markus, T., J.C. Stroeve, and J. Miller (2009). Recent changes in Arctic sea ice melt onset, freezeup, and melt season length, *J. Geophys. Res.*, 114, C12024, doi:10.1029/2009JC005436.

Maslanik, J. (1992). Effects of weather on the retrieval of sea ice concentration and ice type from passive microwave data. *Int. J. Remote Sens.*, 13(1): 37-54.

Meier, W.N., M. Van Woert, and C. Bertoia (2001). Evaluation of operational SSM/I ice concentration algorithms. *Ann. Glaciol.*, 33: 102-108.

Meier, W.N., T. Maksym, and M. Van Woert (2003). Evaluation of Arctic operational passive microwave products: A case study in the Barents Sea during October 2001. “Ice in Environment: Proceedings of the 16th Internatinal Association of Hydraulic Engineering and Research”, Dunedin, NZ, 2-6 Dec. 2002, vol. 3:213-222.

Meier, W.N. (2005). Comparison of passive microwave ice concentration algorithm retrievals with AVHRR imagery in Arctic peripheral seas. *IEEE Trans. Geosci. Remote Sens*., 43(6): 1324-1337.

Meier, W.N., and S.J.S. Khalsa (2011). Intersensor calibration between F-13 SSM/I and F-17 SSMIS Near-Real-Time Sea Ice Estimates. Geoscience and Remote Sensing 49(9): 3343-3349.

Meier, W.N., G. Peng, D.J. Scott, M.H. Savoie (2014). Verification of a new NOAA/NSIDC passive microwave sea-ice concentration climate record, Polar Research, 33, doi:/10.3402/polar.v33.21004.

NAS (2004). Climate data records from environmental satellites: Interim report, National Academies of Science (NAS), National Academies Press, Washington, D.C., 150 pp.

Oelke, C. (1997). Atmospheric signatures in sea-ice concentration estimates from passive microwaves: Modelled and observed. *Int. J. Remote Sens*., 18(5): 1113-1136.

Ozsoy-Cicek, B., H. Xie, S.F. Ackley, and K. Ye (2009). Antarctic summer ice concentrations and extent: Comparison of ODEN 2006 ship observations and NIC sea ice charts. *The Cryosphere*, 3: 1-9.

Ozsoy-Cicek, B., S.F. Ackley, A. Worby, H. Xie, and J. Lieser (2011). Antarctic sea-ice extents and concentrations: Comparison of satellite and ship measurements from International Polar Year cruises. *Ann. Glaciol*., 52(57): 318-326.

Partington, K.C. (2000). A data fusion algorithm for mapping sea-ice concentrations from Special Sensor Microwave/Imager data. *IEEE Trans. Geosci. Remote Sens*., 38(4): 1947-1958.

Peng, G., W.N. Meier, D.J. Scott, and M.H. Savoie (2013). A long-term and reproducible passive microwave sea ice concentration data record for climate studies and monitoring, Earth Sys. Sci. Data, 5, 311-318, doi:10.5194/essd-5-311-2013.

Scambos, T. A., J. A. Bohlander, C. A. Shuman, and P. Skvarca (2004). Glacier acceleration and thinning after ice shelf collapse in the Larsen B embayment, Antarctica. *Geophysical Research Letters*. doi:10.1029/2004GL020670.

Smith, D.M. (1998). Observation of perennial Arctic sea ice melt and freeze-up using passive microwave data, *J. Geophys. Res.*, 103(C12), 27753-27769.

Spreen, G., L. Kaleschke, and G. Heygster (2008). Sea ice remote sensing using AMSR-E 89-GHz channels, /J. Geophys. Res./, 113, C02S03, doi:10.1029/2005JC003384.

Steffen, K., J. Key, D.J. Cavalieri, J. Comiso, P. Gloersen, K. St. Germain, and I. Rubinstein (1992). The estimation of geophysical parameters using passive microwave algorithms, in “Microwave Remote Sensing of Sea Ice.” F.D. Carsey, ed., *American Geophysical Union Monograph* 68, Washington, DC:201-231.

Wentz F. J. (1997). A well-calibrated ocean algorithm for SSM/I. *J. Geophys. Res*., 102(C4): 8703-8718.

Willmes, S., C. Haas, M. Nicolaus, and J. Bareiss (2009). Satellite microwave observations of the interannual variability of snowmelt on sea ice in the Southern Ocean. *J. Geophys. Res.*, 114, C03006, doi:10.1029/2008JC004919.

Zwally, H.J., J.C. Comiso, C.L. Parkinson, W.J. Campbell, F.D. Carsey, and P. Gloersen (1983). Antarctic sea ice 1973-1976 from satellite passive microwave observations. *NASA Spec. Publ*., 459, 206 pp.